I.O.S.

VERTICAL PROFILES OF WIND-INDUCED CURRENT

BY

N.S. HEAPS & J.E. JONES

REPORT NO. 238

1987

NATURAL ENVIRONMENT RESEARCH COUNCIL

INSTITUTE OF OCEANOGRAPHIC SCIENCES

INSTITUTE OF OCEANOGRAPHIC SCIENCES

Wormley, Godalming, Surrey, GU8 5UB.

(042 - 879 - 4141)

(Director: Dr A.S. Laughton FRS)

Bidston Observatory,

Birkenhead, Merseyside, L43 7RA.

(051 - 653 - 8633)

When citing this document in a bibliography the reference should be given as follows:-

HEAPS, N.S. & JONES, J.E. 1987 Vertical profiles of wind-induced current. *Institute of Oceanographic Sciences, Report*, No. 238, 51pp.

INSTITUTE OF OCEANOGRAPHIC SCIENCES

BIDSTON

Vertical profiles of wind-induced current

by

*N.S. Heaps and J.E. Jones

I.O.S. Report No. 238

March 1987

**Dr Norman S Heaps died on 26 June 1986*

CONTENTS

ABSTRACT

Ekman-type current profiles are constructed for five positions in the North Sea and for a range of wind speeds between 5 and 40 ms^{-1}. Their application to determine the vertical distribution of extreme surge current is described. The extent to which logarithmic surface and bottom boundary layers might influence the calculated profiles is investigated.

1. Introduction

The purpose of the present work is to provide some simple profiles of wind-induced current to enable designers of offshore structures in the North Sea to assess the likely variations of surge current through the vertical in extreme storm conditions. It is assumed that extreme values of depth-averaged surge current are available from the continental shelf model (Flather 1984).

The simplifying assumptions associated with Ekman's theory are made. In particular, vertical eddy viscosity is assumed to be a constant and its value is expressed in terms of wind speed by empirical formulae of generally uncertain validity. However, those formulae are probably among the best presently known. Allowance is made for the influence of the tides on the eddy viscosity, mean spring conditions being assumed. The profiles apply to steady-state flow and therefore dynamical effects which might occur in rapidly changing meteorological circumstances are excluded.

The influence of logarithmic surface and bottom boundary layers on the Ekman profiles is investigated. It turns out that the layers are relatively thin (of thickness less than one metre) for wind speeds greater than 15 ms^{-1}. However, the uncertainty concerning the nature of the surface conditions is very considerable at the present time. More advanced theory is needed to link the surface and bottom boundary layer effects to the motion of the interior fluid in a unified rotating dynamical system. Regrettably, the parameters of such a unified system would again possess a significant degree of uncertainty.

It must be emphasised that the outlook of this paper is a practical one, aimed at providing some specific current profiles for use in engineering design. Full details of the derivation of the profiles are given in order to expose the various assumptions which have been made. The approach is a simple one by intention; more sophisticated analyses have, for the time being, been deferred. In any case, with the fundamental uncertainty about turbulence conditions through the vertical water column in storm conditions it seems unlikely that the use of more complicated mathematical formulations would at this stage lead to any more reliable results.

This work was carried out during the current revision of the 'Meteorological and Oceanographic design parameters' section of the Department of Energy publication 'Offshore installations : guidance on design and construction' and when the associated support document was being written. Alternative approaches to estimating current profiles ranging from power and logarithmic laws to three-dimensional modelling are contained within both documents.

2. Ekman theory

Let x, y, z denote Cartesian coordinates forming a left-handed set in which x, y are measured in the horizontal plane of the sea surface and z is depth below that surface (figure 1),

u, v the components of horizontal current at depth z in the directions of increasing x, y,

f the geostrophic coefficient (equal to $2\omega \sin\lambda$ where ω denotes the angular speed of the Earth's rotation and λ the latitude), regarded as a constant,

μ the coefficient of vertical eddy viscosity, also regarded as a constant.

Then, after Ekman (1905), wind-induced currents through the vertical water column from sea surface to sea bed satisfy the dynamical equations

$$\mu \frac{d^2u}{dz^2} = -fv \quad , \quad \mu \frac{d^2v}{dz^2} = fu \quad . \tag{1}$$

These are derived assuming a homogeneous sea, horizontal uniformity, and a steady wind stress. They may be combined to give the well-known equation

$$\frac{d^2w}{dz^2} = \frac{\pi^2(1+i)^2}{D^2} w \tag{2}$$

where horizontal current is expressed in the complex form :

$$w = u + iv \tag{3}$$

and

$$D = \pi\left(2\mu/f\right)^{1/2} . \tag{4}$$

Supposing that the wind stress is of magnitude T and acts in the y-direction, the surface stress condition is

$$-\rho\mu \frac{dw}{dz} = iT \quad \text{at} \quad z = 0 \quad . \tag{5}$$

At the sea bed, adopting a linear law of bottom friction, with a constant coefficient k , we have

$$-\rho\mu \frac{dw}{dz} = k\rho w \quad \text{at} \quad z = h \ . \tag{6}$$

Here ρ denotes the density of the sea water and h the total depth.

Solving (2), subject to (5) and (6), yields

$$w = \frac{\pi T}{\rho f D}\left[\frac{a\alpha(1+i)\sinh\{(1+i)a\eta\} + 2i\cosh\{(1+i)a\eta\}}{a\alpha\cosh\{(1+i)a\} + (1+i)\sinh\{(1+i)a\}}\right] \tag{7}$$

where :

$$a = \frac{\pi h}{D} \ , \quad \alpha = \frac{2k}{fh} \ , \quad \eta = 1 - \frac{z}{h} \ . \tag{8}$$

Then, taking real and imaginary parts in (7), produces the horizontal components of current in the form :

$$u = \beta p/d \ , \quad v = \beta q/d \tag{9}$$

in which

$$\beta = \pi T/\rho f D \tag{10}$$

$$\begin{aligned} d = {} & a^2\alpha^2(\cosh^2 a\cos^2 a + \sinh^2 a\sin^2 a) \\ & + 2a\alpha(\sinh a\cosh a - \sin a\cos a) \\ & + 2(\sinh^2 a\cos^2 a + \cosh^2 a\sin^2 a) \end{aligned} \tag{11}$$

$$p = a^2\alpha^2 \Big\{ \sinh ay \cos ay \,(\cosh a \cos a + \sinh a \sin a) - \cosh ay \sin ay \,(\cosh a \cos a - \sinh a \sin a) \Big\}$$

$$+ 2a\alpha \Big\{ \sinh ay \cos ay \sinh a \cos a + \cosh ay \sin ay \cosh a \sin a + \cosh ay \cos ay \sinh a \sin a - \sinh ay \sin ay \cosh a \cos a \Big\}$$

$$+ 2 \Big\{ \cosh ay \cos ay \,(\sinh a \cos a + \cosh a \sin a) + \sinh ay \sin ay \,(\cosh a \sin a - \sinh a \cos a) \Big\} \tag{12}$$

and

$$q = a^2\alpha^2 \Big\{ \sinh ay \cos ay \,(\cosh a \cos a - \sinh a \sin a) + \cosh ay \sin ay \,(\cosh a \cos a + \sinh a \sin a) \Big\}$$

$$+ 2a\alpha \Big\{ - \sinh ay \cos ay \cosh a \sin a + \cosh ay \sin ay \sinh a \cos a + \cosh ay \cos ay \cosh a \cos a + \sinh ay \sin ay \sinh a \sin a \Big\}$$

$$+ 2 \Big\{ \cosh ay \cos ay \,(\sinh a \cos a - \cosh a \sin a) + \sinh ay \sin ay \,(\cosh a \sin a + \sinh a \cos a) \Big\} . \tag{13}$$

Using (7), the depth-mean current comes out to

$$\bar{w} = \bar{u} + i \bar{v}$$

$$= \frac{1}{h} \int_0^h w \, dz$$

$$= \frac{\pi T}{\rho f D a} \left[\frac{a\alpha \left(\cosh \{ (1+i)a \} - 1 \right) + (1+i) \sinh \{ (1+i)a \}}{a\alpha \cosh \{ (1+i)a \} + (1+i) \sinh \{ (1+i)a \}} \right] . \tag{14}$$

Taking real and imaginary parts in (14) leads to the depth-mean components of current expressed in the form :

$$\bar{u} = \beta p_1 / ad \quad , \quad \bar{v} = \beta q_1 / ad \tag{15}$$

in which

$$\begin{aligned} p_1 = {} & a^2 \alpha^2 \left(\cosh^2 a \cos^2 a + \sinh^2 a \sin^2 a - \cosh a \cos a \right) \\ & + a\alpha \left(2 \sinh a \cosh a - 2 \sin a \cos a - \sinh a \cos a + \cosh a \sin a \right) \\ & + 2 \left(\sinh^2 a \cos^2 a + \cosh^2 a \sin^2 a \right) \end{aligned} \tag{16}$$

and

$$q_1 = a^2 \alpha^2 \sinh a \sin a + a\alpha \left(\cosh a \sin a + \sinh a \cos a \right) . \tag{17}$$

3. Vertical profiles

At any location, equations (9) and (15) may be used to calculate the vertical profiles of

$$u \, , \, v \tag{18}$$

and their departures from the mean :

$$u - \bar{u} \quad , \quad v - \bar{v} \quad . \tag{19}$$

Note that v is the current component in the direction of the wind, with u to the right of it (figure 1).

Profiles may also be determined for the magnitude of the resultant current at any depth

$$V = (u^2 + v^2)^{1/2} \tag{20}$$

and the magnitude of the departure of this resultant from the depth-mean current :

$$V_\delta = \left[(u - \bar{u})^2 + (v - \bar{v})^2 \right]^{1/2} \quad . \tag{21}$$

Wind stress in the calculations may be determined from a square law :

$$T = c_D \rho_A W^2 \tag{22}$$

where W denotes the wind speed, ρ_A the density of the air and c_D a drag coefficient. Then β from (10) may be evaluated using

$$\beta = \frac{\pi c_D \rho_A W^2}{\rho f D} \quad . \tag{23}$$

4. Frictional parameters

Using a result due to Svensson (1979), and putting together arguments given by Csanady (1976) and Heaps (1984), for wind-driven flow we take

$$\left.\begin{aligned} \mu = \mu_W &= 0.065\, h\, u_* && h \leq h_E \\ &= 0.026\, u_*^2 / f && h \geq h_E \end{aligned}\right\} \tag{24}$$

where

$$u_* = (T/\rho)^{1/2} = (c_D \rho_A / \rho)^{1/2} W \tag{25}$$

and

$$h_E = 0.4\, u_* / f \quad . \tag{26}$$

For tidal flow we take

$$\mu = \mu_T = \tfrac{1}{2} \kappa \,(a_T^2 + b_T^2) \tag{27}$$

where a_T , b_T denote, respectively, the semi-major and semi-minor axes of the tidal current ellipse and $\kappa = 0.2\ s^{-1}$. Equation (27) is obtained by averaging over a tidal cycle the form for μ used by Davies and Furnes (1980) when computing M_2 tidal currents in the North Sea, namely the form $\mu = \kappa\, (\bar{u}^2 + \bar{v}^2)$.

For a combined wind-driven and tidal flow it is tentatively assumed that

$$\mu = \max\, (\mu_W , \mu_T) \tag{28}$$

where max indicates that the maximum of μ_W and μ_T is taken.

Setting $kh/\mu = 2$ as in Heaps (1974), k is determined from

$$k = 2\mu / h \quad . \tag{29}$$

5. North Sea currents

Calculations of the vertical profiles associated with wind-induced currents were done for five positions in the North Sea : N_1, N_2, N_3, N_4, N_5 marked in figure 2. The depths at these positions vary between 29m at N_1, in the south, to 177m at N_5, in the north. Table 1 lists the geographical coordinates, depth, and tidal parameters a_T, b_T and μ_T at mean springs, M_2+S_2. The values of μ_T come from (27).

For the calculation of μ_W at the various positions we took

$$\left.\begin{aligned} \rho_A &= 0.00125 \quad gcm^{-3} \\ \rho &= 1.027 \quad gcm^{-3} \\ f &= 1.18 \times 10^{-4}\ s^{-1} \end{aligned}\right\} \tag{30}$$

and, from Smith and Banke (1975),

$$c_D = 10^{-3}\ (0.63 + 0.066\,W) \tag{31}$$

where the wind speed W is measured in ms^{-1}. The geostrophic coefficient, f, corresponds to $\lambda = 54^{\circ}$, a representative latitude for British waters. Then, from (25) and (26) :

$$u_* = 0.11032\ W\ (0.63 + 0.066\,W)^{\frac{1}{2}} \tag{32}$$

$$h_E = 33.9\ u_* \tag{33}$$

where u_* is in cms^{-1} and h_E in metres. For the range of wind speeds :

$$W = 5\ (5)\ 40\ ms^{-1} \tag{34}$$

the u_* and h_E are listed in Table 2. The μ_W calculated using (24) are presented in Table 3 for the various positions and wind speeds. The corresponding μ values, derived from (28) with μ_T for mean springs given by Table 1, are presented in Table 4. Note that the tidal contribution to μ is only important at N_1 and to a lesser extent at N_3. Values of k, obtained using (29), are presented in Table 5.

Employing the preceding values in (9) and (15), the vertical profiles of

(a) $u\,, \quad v\,, \quad V = (u^2+v^2)^{1/2}$

(b) $u - \bar{u}$

(c) $v - \bar{v}$

(d) $V_s = \left[(u-\bar{u})^2 + (v-\bar{v})^2 \right]^{1/2}$

are plotted for each position N_1 to N_5 in figures 3 to 7 respectively. Each diagram shows curves for the range of wind speeds W = 5 (5) 40 ms^{-1}.

6. Surface and bottom logarithmic boundary layers

It seems important to estimate the thicknesses of the logarithmic boundary layers assumed to exist adjacent to the sea surface and sea bed. Within those layers, the profiles shown in figures 3 to 7 based on Ekman's theory will not apply.

The vertical distribution of horizontal current in a non-rotating surface logarithmic boundary layer (Bowden 1983, p. 134) may be written

$$\left.\begin{aligned} u &= 0 \\ v &= \alpha W - (u_*/\kappa_0)\log(z/z_0) \end{aligned}\right\} \qquad (35)$$

where α is the wind factor, z_0 the roughness length, and κ_0 Von Karman's constant. Note that the currents lie in the wind direction. The following values are taken :

$$\left.\begin{aligned} \alpha &= 0.03 \\ z_0 &= 0.001 \text{ m} \\ \kappa_0 &= 0.40. \end{aligned}\right\} \qquad (36)$$

Figure 8(a) illustrates how the logarithmic curve reduces from a surface value of V_s' ($v = \alpha W = V_s'$ at $z = z_0$) and cuts the Ekman profile V where $z = z_a$, $V = V_a$. This assumes that $V_s' > V_s$, where $V = V_s$ at $z = 0$ on the Ekman profile.

Table 6 gives the values of V_s , V_s' , V_a and z_a determined (numerically) for the positions N_1 to N_5 and the various wind speeds from 10 to 40 ms^{-1}. Gaps are left in the Table where $V_s' < V_s$. It is evident that the thickness of the boundary layer, taken as z_a , does not exceed 2.31m - its value at N_1 for $W = 10$ ms^{-1}. For $W \geqslant 15$ ms^{-1}, the thickness is less than 0.5m. Thus, for the higher wind speeds, the logarithmic surface boundary layer scarcely affects the Ekman profiles presented in this paper.

However, Csanady (1984) has suggested that z_0 may be one to two orders of magnitude greater than the value allocated to it in (36). Taking $z_0 = 0.05$m to exemplify such a possibility leads to the values of V_s , V_s' , V_a and z_a in Table 7. Considerably larger values of z_a now appear; in fact the surface boundary layer can be quite thick. For $W = 10$, 15 ms^{-1} the Ekman and logarithmic curves do not even intersect, indicating that the logarithmic variation might affect the entire current profile from sea surface to sea bed. The uncertainty in ζ_0 at the sea surface, caused by the recent proposal by Csanady of a greatly enhanced value, clearly introduces an important uncertainty into the validity of the Ekman profiles of this paper.

For the logarithmic bottom boundary layer, we have

$$V = \frac{u_{*b}}{\kappa_0} \log\left(\frac{Z}{Z_0}\right) \tag{37}$$

where Z is distance measured vertically upwards from the bottom, Z_0 a bottom roughness length, and

$$u_{*b} = \left(\tau_b / \rho\right)^{1/2} . \tag{38}$$

Here, τ_b denotes the bottom stress given in the present analysis by

$$\tau_b = k\rho\left(u_b^2 + v_b^2\right)^{1/2} \tag{39}$$

where u_b , v_b denote the values of u , v at the sea bed. Combining (37), (38) and (39) yields

$$V = \frac{k^{1/2}\left(u_b^2 + v_b^2\right)^{1/4}}{\kappa_0} \log\left(\frac{Z}{Z_0}\right) . \tag{40}$$

Using Z_0 given in Table 8, estimated by R.L. Soulsby (private communication), the logarithmic curve (40) has been evaluated and its intersection point with the Ekman profile at $Z = Z_c$, $V = V_c$ determined. Figure 8(b) illustrates this behaviour; $V = V_b$ at the sea bottom on the Ekman profile. Table 9 gives V_b , V_c , Z_c for the various positions N_1 to N_5 and the various wind speeds between 10 and 40 ms^{-1}. It is evident that the thickness of the bottom boundary layer, taken as Z_c , is everywhere less than about 0.1m and therefore the layer has only a small perturbing influence on the Ekman profiles.

The dynamical inconsistency in the above discussion between the non-rotating logarithmic boundary layers and the rotating Ekman flow regime is recognised. However, the two concepts are regularly used and are retained together here because of that.

The roughness lengths ζ_0 , Z_0 are clearly key parameters in determining how far the boundary influences penetrate vertically into the main body of the sea. The bottom roughness length Z_0 has been related to various types of sea-bed sedimentation (Soulsby 1983) and the values in Table 8 were derived on this basis. Estimation of the surface roughness length is much more uncertain. The value taken in (36) is consistent with the arguments given by Madsen (1977) and the laboratory experiments of Wu (1975).

Taking α = 0.03 in (36) indicates that the surface current is assumed to be 3% of the surface wind speed, a generally applicable result (Pearce and Cooper 1981).

7. Advice

The use of the wind-induced current profiles in figures 3 - 7 for the estimation of the distribution of extreme surge current through depth is now outlined.

A known extreme depth-integrated surge current may be incremented through depth by

$$V - (\bar{u}^2 + \bar{v}^2)^{1/2}$$

to yield estimates of the corresponding surge current extremes at various depths. The wind speed W should be selected as the maximum expected value based on meteorological records. Here, V, $\bar{u}$, $\bar{v}$ come from figures 3(a) - 7(a). Incrementing by V_ζ is also possible, tending however to yield overestimates of the extremes. The V_ζ comes from figures 3(d) - 7(d).

Known components of depth-integrated surge current may be incremented by $u-\bar{u}$, $v-\bar{v}$ (given by figures 3(b,c) - 7(b,c)) to yield estimates of the corresponding depth variations. Wind direction as well as magnitude is needed here to resolve the prescribed components in the wind direction and at right angles to it before incrementation. If the wind direction associated with the surge components is unknown, then a range of profiles relating to different wind directions could be evaluated.

Logarithmic boundary layers may exist at the sea surface and sea bed as explained in §6. For the higher wind speeds those layers are likely to be very thin - less than a metre thick for wind speeds greater than 15 ms^{-1}. On these grounds, the Ekman current profiles may be considered to apply through most of the vertical water column in storm conditions. However, with uncertainties about the thickness of the surface layer, this has to be regarded as a tentative conclusion.

References

BOWDEN, K.F., 1983. Physical Oceanography of Coastal Waters, Ellis Horwood, Chichester, 302pp.

CSANADY, G.T., 1976. Mean circulation in shallow seas. Journal of Geophysical Research, 81, 5389-5399.

CSANADY, G.T., 1984. The free surface turbulent shear layer. Journal of Physical Oceanography, 14, 402-411.

DAVIES, A.M. AND FURNES, G.K., 1980. Observed and computed M_2 tidal currents in the North Sea. Journal of Physical Oceanography, 10, 237-257.

EKMAN, V.W., 1905. On the influence of the Earth's rotation on ocean currents. Arkiv för Matematik, Astronomi och Fysik, 2(11), 1-52.

FLATHER, R.A., 1984. A numerical model investigation of the storm surge of 31 January and 1 February 1953 in the North Sea. Quarterly Journal of the Royal Meteorological Society, 110, 591-612.

HEAPS, N.S., 1974. Development of a three-dimensional numerical model of the Irish Sea. Rapp. P.-v. Réun. Cons. perm. int. Explor. Mer, 167, 147-162.

HEAPS, N.S., 1984. Vertical structure of current in homogeneous and stratified waters. pp. 153-207 in, Hydrodynamics of Lakes, ed. K. Hutter, Springer-Verlag, 341pp.

MADSEN, O.S., 1977. A realistic model of the wind-induced Ekman boundary layer. Journal of Physical Oceanography, 7, 248-255.

PEARCE, B.R. AND COOPER, C.K., 1981. Numerical circulation model for wind-induced flow. Journal of the Hydraulics Division, Proceedings of the American Society of Civil Engineers, 107(HY3), 285-302.

SMITH, S.D. AND BANKE, E.G., 1975. Variation of the sea surface drag coefficient with wind speed. Quarterly Journal of the Royal Meteorological Society, 101, 665-673.

SOULSBY, R.L., 1983. The bottom boundary layer of shelf seas. pp 189-266 in, Physical Oceanography of Coastal and Shelf Seas, ed. B. Johns, Elsevier, Amsterdam.

SVENSSON, U., 1979. The structure of the turbulent Ekman layer. Tellus, 31, 340-350.

WU, J., 1975. Wind-induced drift currents. Journal of Fluid Mechanics, 68, 49-70.

Position	Coordinates	h (m)	a_T (cms^{-1})	b_T (cms^{-1})	μ_T (cm^{2}s^{-1})
N_1	53° 10'N, 2° 15'E	29	86	17	768
N_2	56° 30'N, 2° 45'E	77	24	2	58
N_3	57° 50'N, 1° 15'E	97	32	5	105
N_4	60° 10'N, 2° 15'E	143	16	6	29
N_5	61° 30'N, 1° 15'E	177	8	5	9

Table 1. Geographical positions, depth and tidal parameters at mean springs (M_2 + S_2) relating to N_1, N_2, N_3, N_4, N_5.

W ms^{-1}	u_* cms^{-1}	h_E m
5	0.5405	18.3
10	1.253	42.5
15	2.106	71.4
20	3.081	104.4
25	4.164	141.2
30	5.347	181.3
35	6.621	224.4
40	7.980	270.5

Table 2. u_* and h_E for various W

$W\ (ms^{-1})$	N_1	N_2	N_3	N_4	N_5
5	64	64	64	64	64
10	236	346	346	346	346
15	397	977	977	977	977
20	581	1542	1943	2092	2092
25	785	2084	2626	3821	3821
30	1008	2676	3371	4970	6152
35	1248	3314	4174	6154	7617
40	1504	3994	5031	7417	9181

Table 3. μ_W in cm^2s^{-1} for the various positions and wind speeds.

W (ms^{-1})	N_1	N_2	N_3	N_4	N_5
5	768	64	105	64	64
10	768	346	346	346	346
15	768	977	977	977	977
20	768	1542	1943	2092	2092
25	785	2084	2626	3821	3821
30	1008	2676	3371	4970	6152
35	1248	3314	4174	6154	7617
40	1504	3994	5031	7417	9181

Table 4. μ in cm^2s^{-1} for the various positions and wind speeds, assuming mean spring tidal conditions.

W (ms^{-1})	N_1	N_2	N_3	N_4	N_5
5	0.52	0.016	0.020	0.008	0.008
10	0.52	0.08	0.08	0.04	0.04
15	0.52	0.26	0.20	0.14	0.12
20	0.52	0.40	0.40	0.30	0.24
25	0.54	0.54	0.54	0.54	0.44
30	0.70	0.70	0.70	0.70	0.70
35	0.86	0.86	0.86	0.86	0.86
40	1.04	1.04	1.04	1.04	1.04

Table 5. k in cms^{-1} for the various positions and wind speeds.

		W (ms^{-1}) →						
		10	15	20	25	30	35	40
N_1	V_s	6.10	17.23	36.88	66.60	95.42	127.29	161.10
	V_s'	30.00	45.00	60.00	75.00	90.00	105.00	120.00
	V_a	5.73	17.14	36.86	66.57	-	-	-
	z_a	2.31	0.20	0.02	0.002	-	-	-
N_2	V_s	7.78	12.85	22.29	36.36	55.10	78.51	106.45
	V_s'	30.00	45.00	60.00	75.00	90.00	105.00	120.00
	V_a	7.35	12.70	22.24	36.33	55.09	78.50	106.41
	z_a	1.38	0.46	0.13	0.041	0.014	0.005	0.002
N_3	V_s	7.77	12.98	19.56	31.43	47.29	67.41	91.96
	V_s'	30.00	45.00	60.00	75.00	90.00	105.00	120.00
	V_a	7.34	12.84	19.50	31.40	47.28	67.40	91.95
	z_a	1.39	0.45	0.19	0.066	0.024	0.010	0.004
N_4	V_s	7.77	13.08	19.00	25.42	37.19	52.35	71.12
	V_s'	30.00	45.00	60.00	75.00	90.00	105.00	120.00
	V_a	7.34	12.94	18.93	25.38	37.17	52.33	71.11
	z_a	1.39	0.44	0.21	0.117	0.052	0.024	0.012
N_5	V_s	7.77	13.06	19.13	25.55	33.06	46.05	62.07
	V_s'	30.00	45.00	60.00	75.00	90.00	105.00	120.00
	V_a	7.34	12.92	19.07	25.51	33.04	46.03	62.06
	z_a	1.39	0.44	0.20	0.116	0.071	0.035	0.018

Table 6. Values of V_s , V_s' , V_a (in cms^{-1}) and z_a (in metres) at positions N_1 to N_5 for various wind speeds; z_0 = 0.001m.

$W\ (ms^{-1}) \rightarrow$

		10	15	20	25	30	35	40
N_1	V_s	6.10	17.23	36.88	66.60	95.42	127.29	161.10
	V_s'	30.00	45.00	60.00	75.00	90.00	105.00	120.00
	V_a	-	-	35.73	65.88	-	-	-
	ζ_a	-	-	1.17	0.12	-	-	-
N_2	V_s	7.78	12.85	22.29	36.36	55.10	78.51	106.45
	V_s'	30.00	45.00	60.00	75.00	90.00	105.00	120.00
	V_a	-	-	18.00	35.05	54.58	78.25	106.33
	ζ_a	-	-	11.67	2.32	0.708	0.252	0.099
N_3	V_s	7.77	12.98	19.56	31.43	47.29	67.41	91.96
	V_s'	30.00	45.00	60.00	75.00	90.00	105.00	120.00
	V_a	-	-	14.17	29.75	46.56	67.06	91.78
	ζ_a	-	-	19.18	3.86	1.29	0.495	0.206
N_4	V_s	7.77	13.08	19.00	25.42	37.19	52.35	71.12
	V_s'	30.00	45.00	60.00	75.00	90.00	105.00	120.00
	V_a	-	-	12.95	23.24	36.11	51.75	70.78
	ζ_a	-	-	22.47	7.21	2.82	1.25	0.589
N_5	V_s	7.77	13.06	19.13	25.55	33.06	46.05	62.07
	V_s'	30.00	45.00	60.00	75.00	90.00	105.00	120.00
	V_a	-	-	13.36	23.34	31.84	45.33	61.64
	ζ_a	-	-	21.32	7.14	3.88	1.84	0.932

Table 7. Values of V_s , V_s' , V_a (in cms^{-1}) and ζ_a (in metres) at positions N_1 to N_5 for various wind speeds; $\zeta_0 = 0.05m$.

N_1	N_2	N_3	N_4	N_5
0.600	0.002	0.002	0.020	0.020

Table 8. Z_o in centimetres at the locations N_1 to N_5

$W \ (ms^{-1}) \rightarrow$

		10	15	20	25	30	35	40
N_1	V_t	1.994	5.636	12.060	21.585	31.091	41.947	53.165
	V_c	2.007	5.645	12.093	21.698	31.280	42.237	53.730
	Z_c	0.01320	0.02244	0.04141	0.07625	0.08769	0.09995	0.10800
N_2	V_t	0.494	2.391	5.516	10.113	16.263	24.187	33.506
	V_c	0.497	2.458	5.570	10.475	16.425	24.384	34.000
	Z_c	0.00005	0.00007	0.00009	0.00012	0.00014	0.00017	0.00020
N_3	V_t	0.216	1.627	4.281	8.032	13.161	19.915	28.080
	V_c	0.220	1.778	4.539	8.386	13.606	20.146	28.111
	Z_c	0.00004	0.00007	0.00008	0.00010	0.00012	0.00014	0.00016
N_4	V_t	0.037	0.588	2.317	5.195	8.870	13.781	19.918
	V_c	0.037	0.596	2.325	5.245	8.934	13.847	19.998
	Z_c	0.00029	0.00046	0.00061	0.00070	0.00084	0.00100	0.00116
N_5	V_t	0.009	0.265	1.414	3.711	6.988	11.026	16.143
	V_c	0.009	0.274	1.419	3.720	7.001	11.041	16.183
	Z_c	0.00024	0.00037	0.00053	0.00064	0.00071	0.00084	0.00097

Table 9. Values of V_t , V_c (in cms^{-1}) and Z_c (in metres) at positions N_1 to N_5 for various wind speeds.

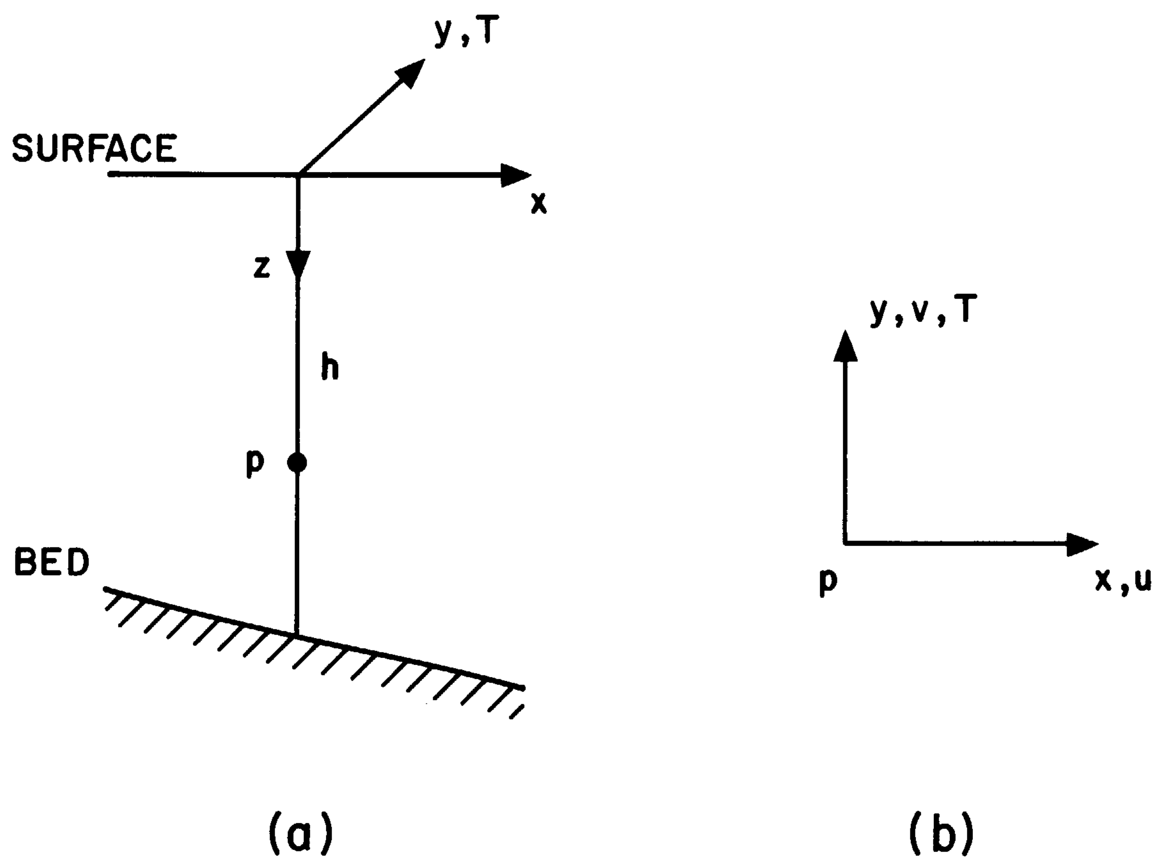

Figure I. (a) Vertical water column between sea surface and sea bed and (b) horizontal planform of currents and wind stress.

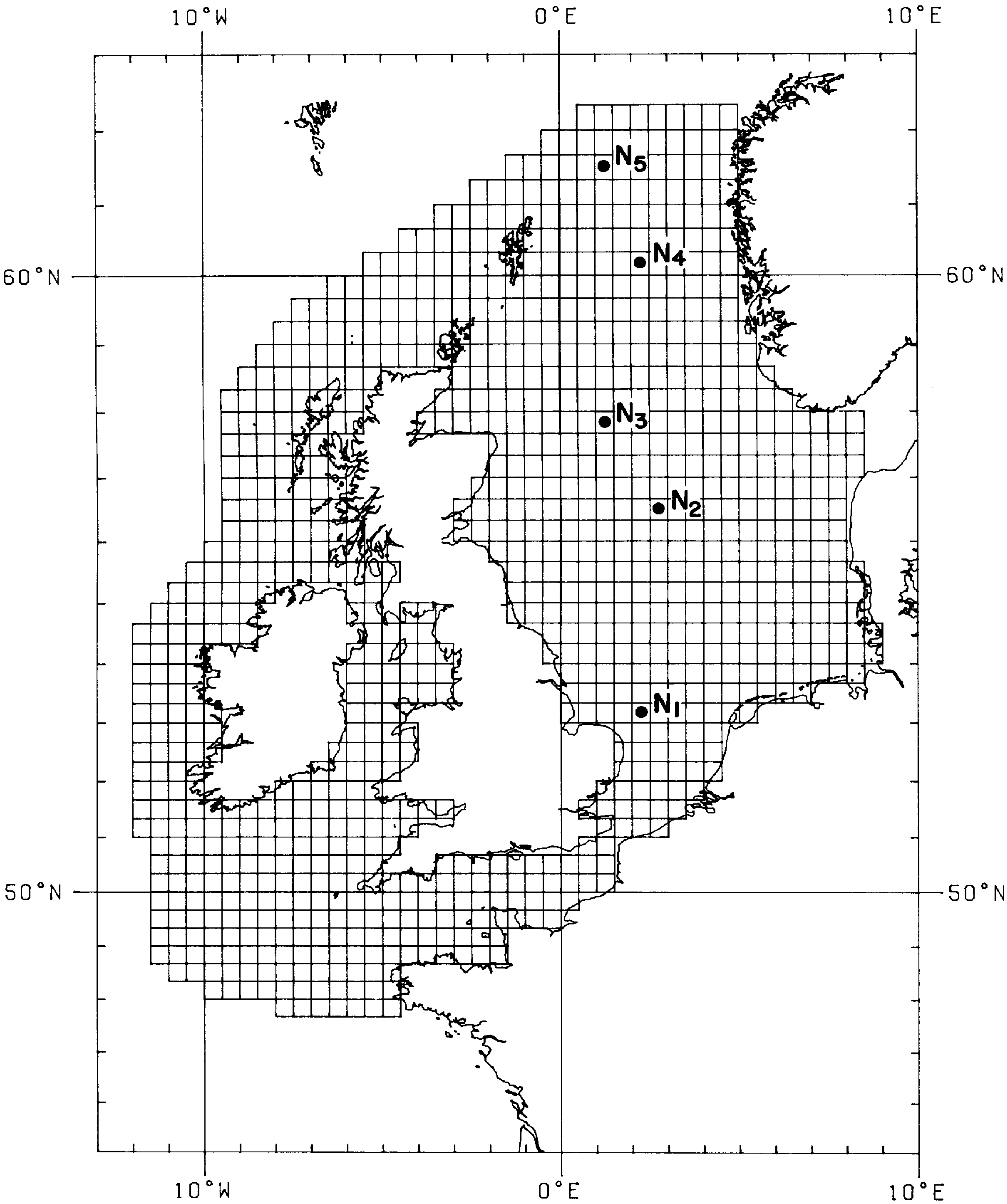

Figure 2. Positions N_1, N_2, N_3, N_4, N_5 marked on the grid of the continental shelf numerical model for tides and storm surges (Flather 1984).

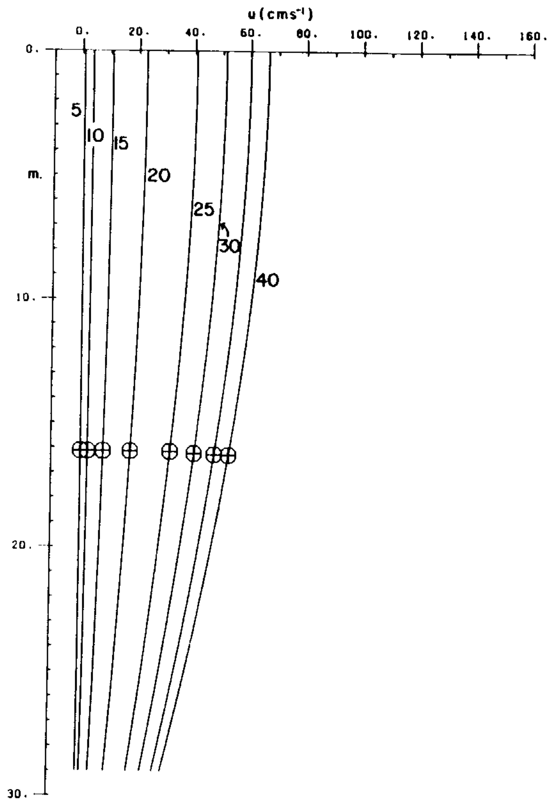

Figure 3 (a)

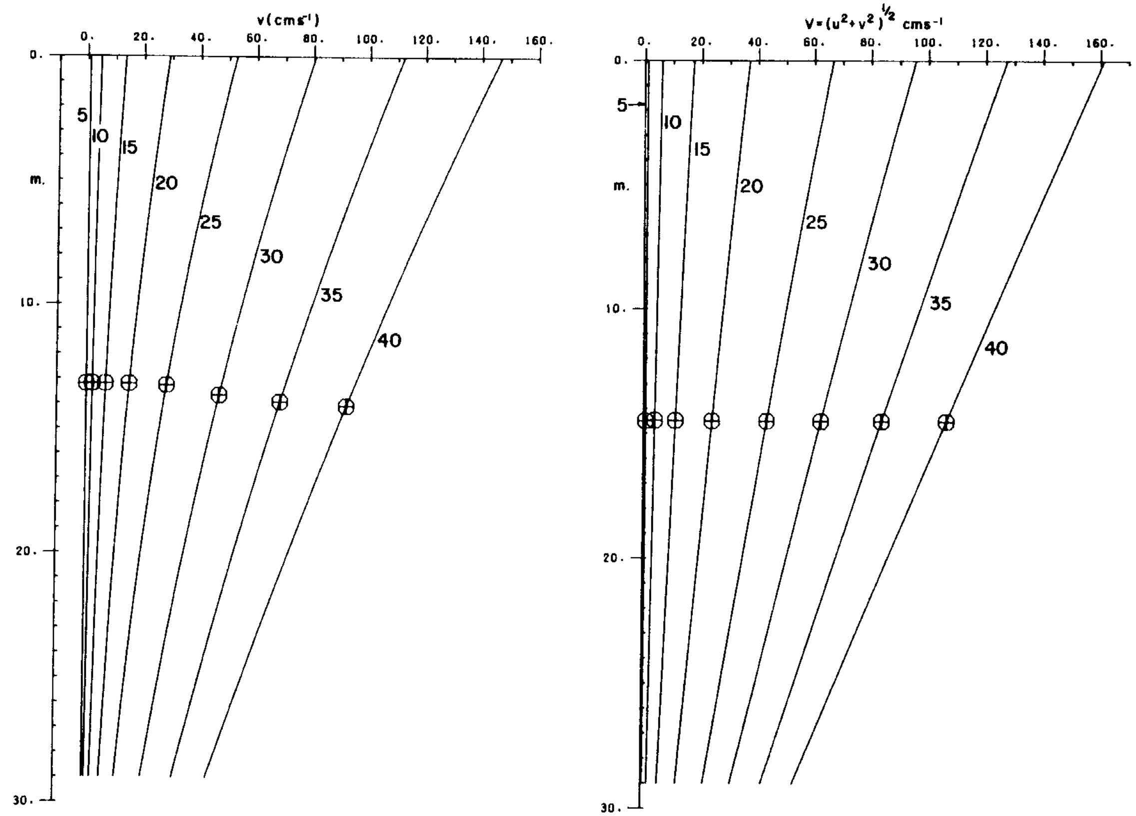

Figure 3 (a – d). Current profiles at position N_1 ; $\oplus$ denotes the depth-mean; for wind speeds 5(5) 40 ms^{-1}.

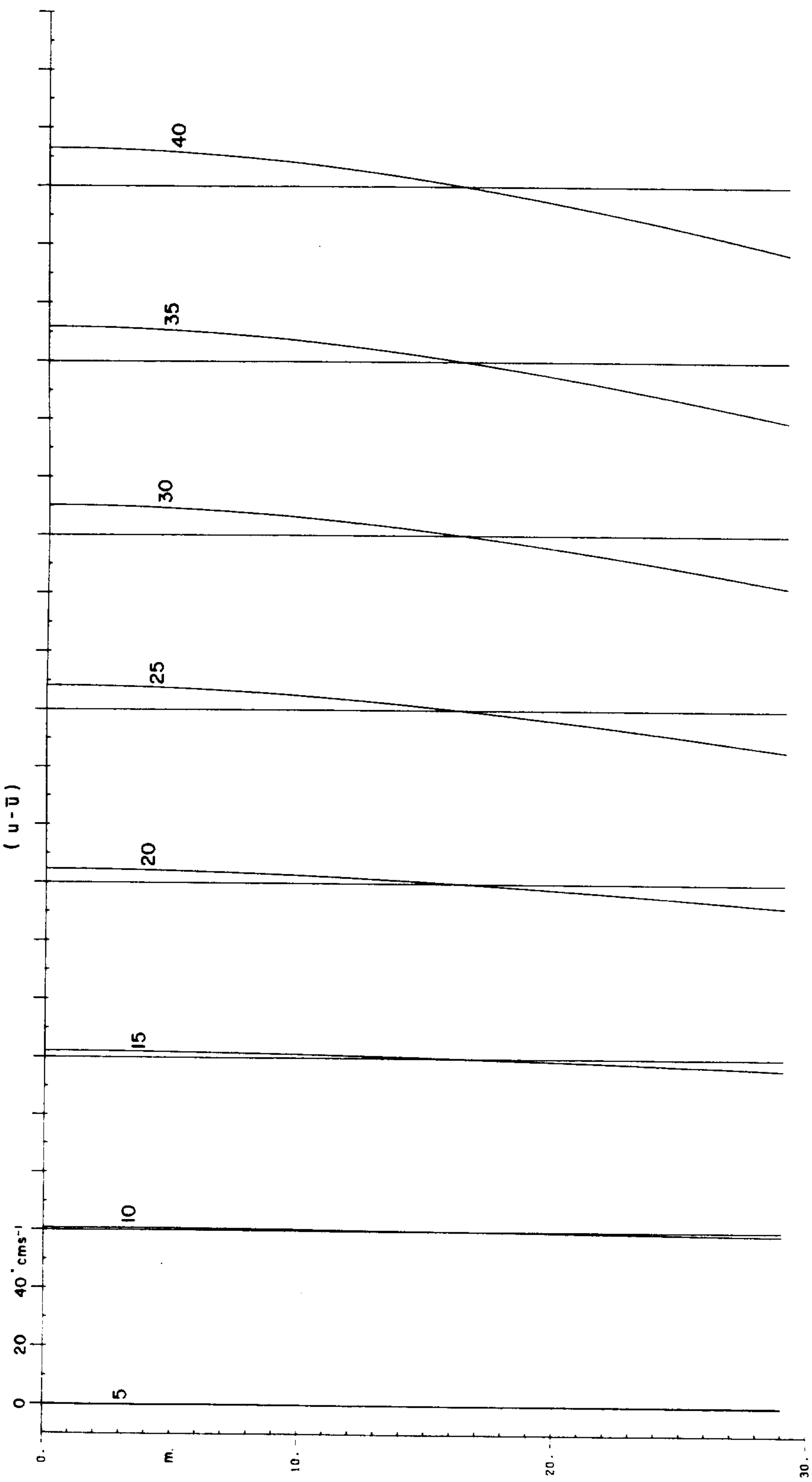

Figure 3(b)

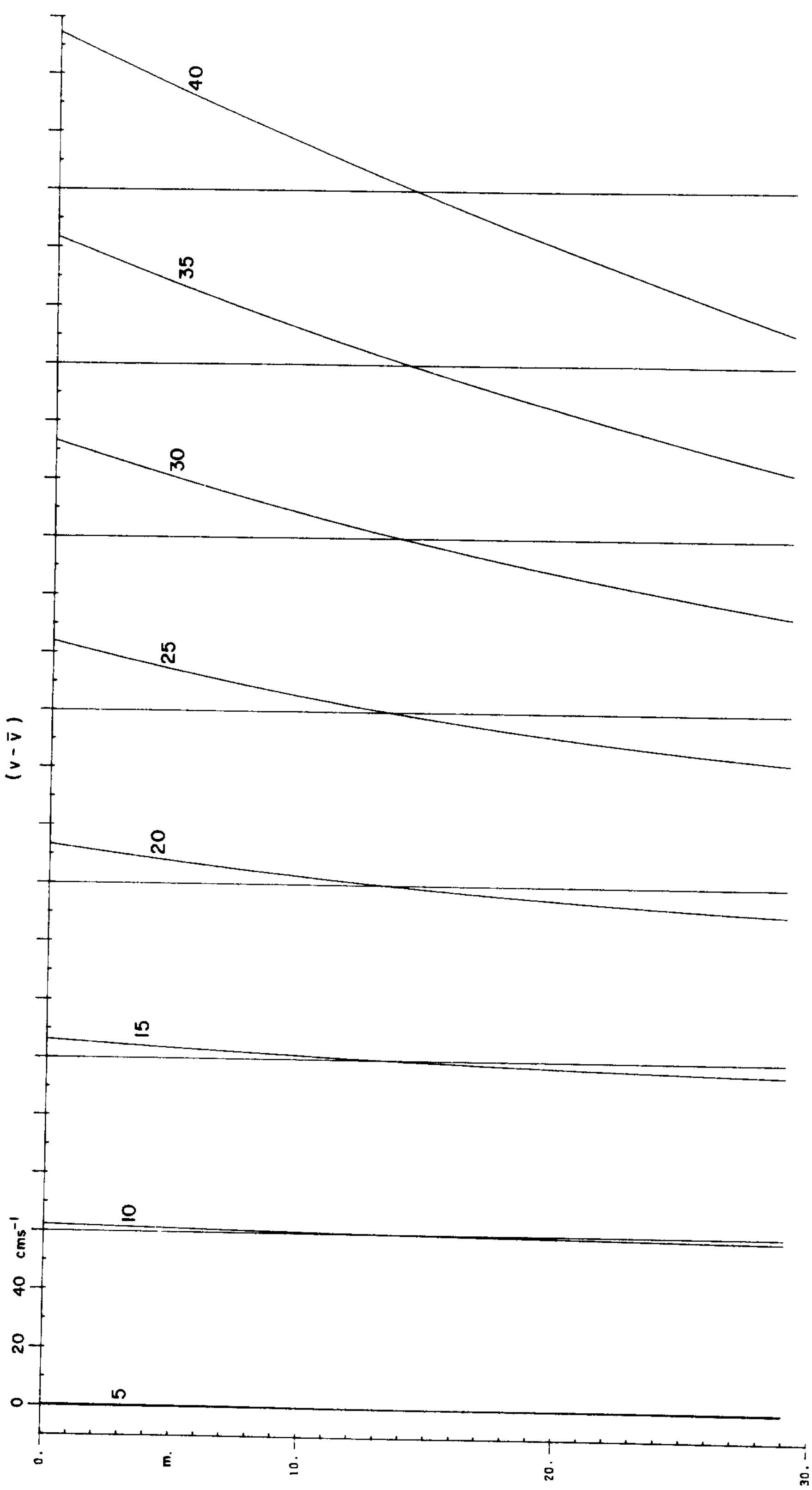

Figure 3(c)

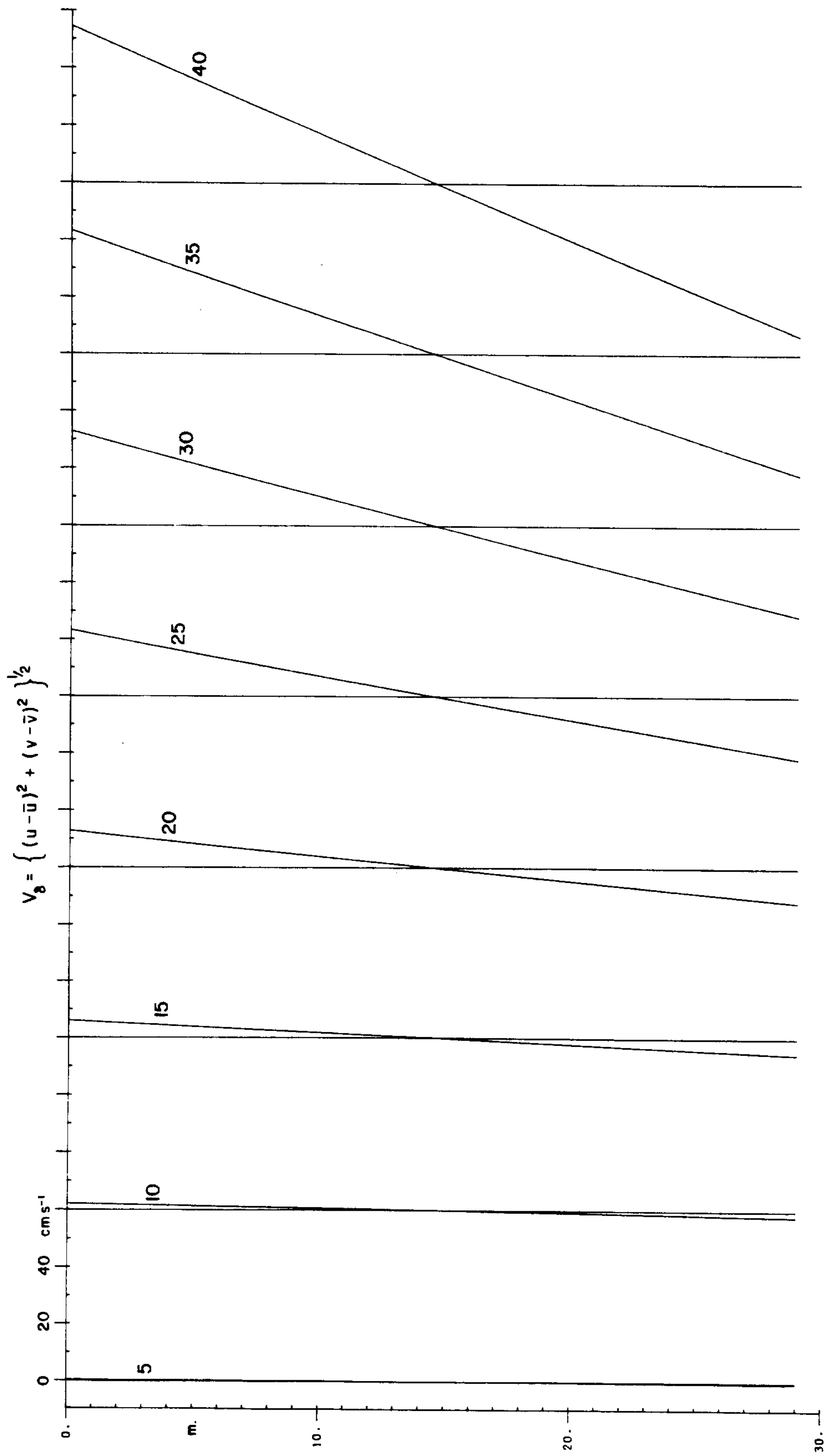

Figure 3(d)

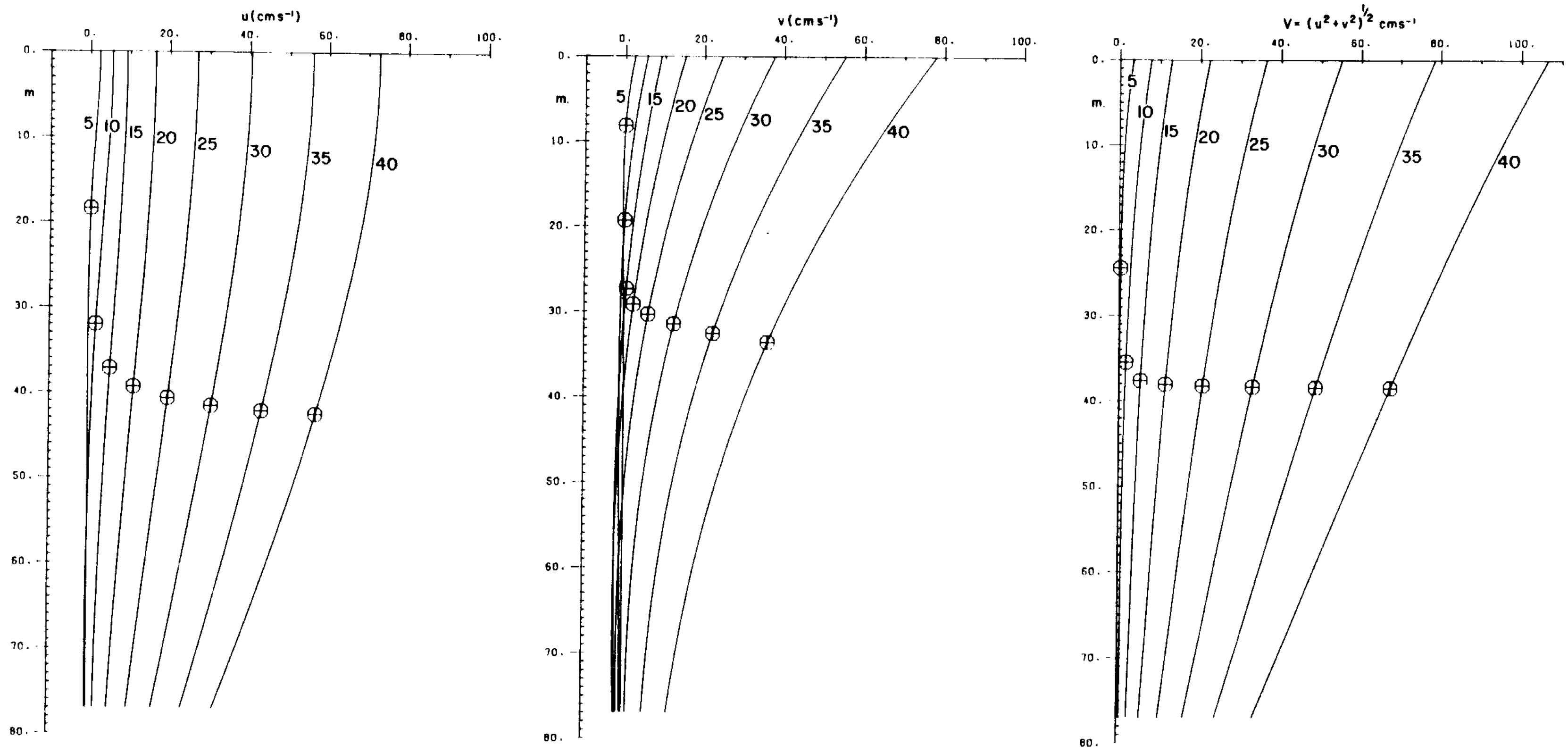

Figure 4(a)

Figure 4 (a-d). Current profiles at position N_2 ; $\oplus$ denotes the depth-mean; for wind speeds 5(5)40 ms^{-1}.

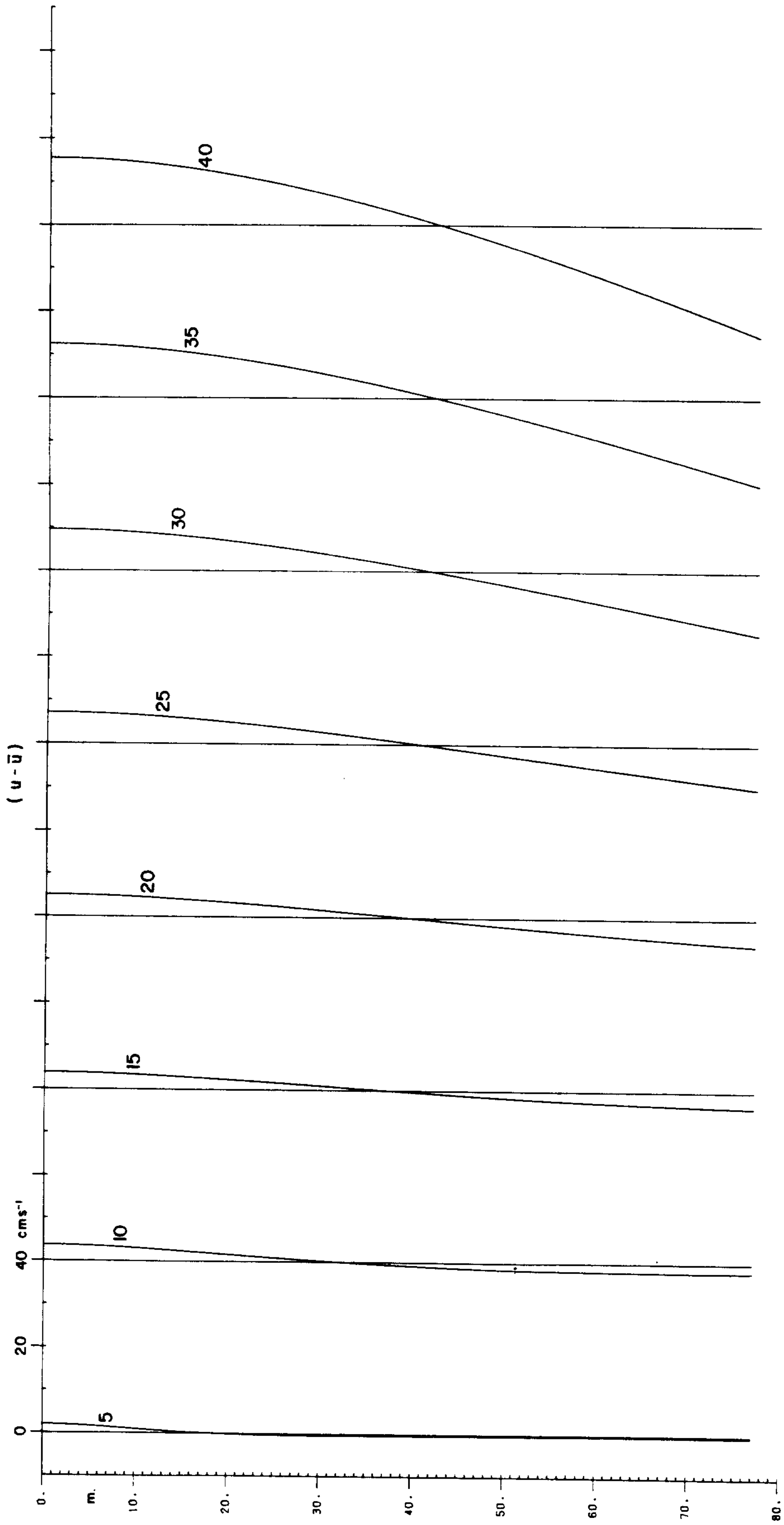

Figure 4(b)

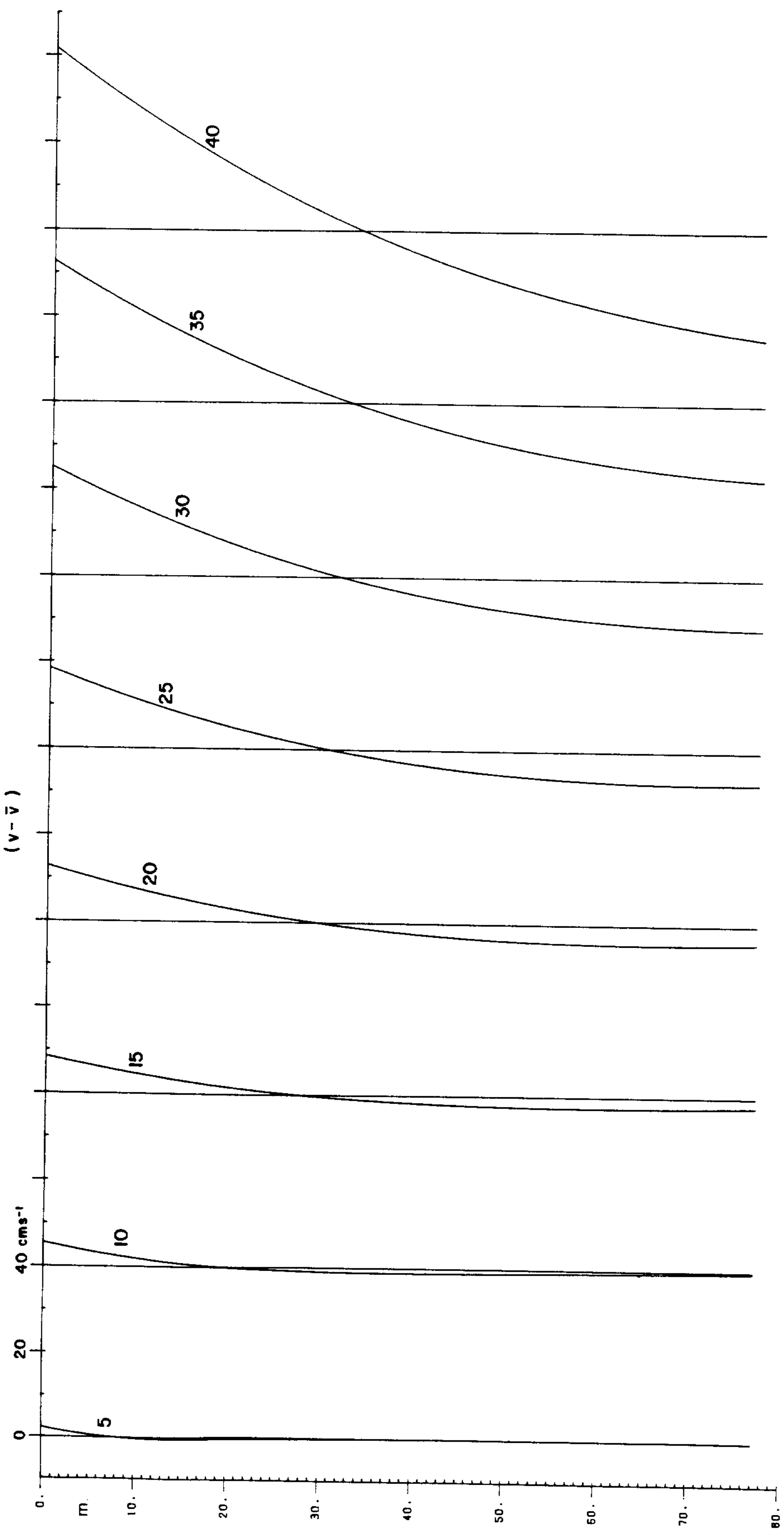

Figure 4 (c)

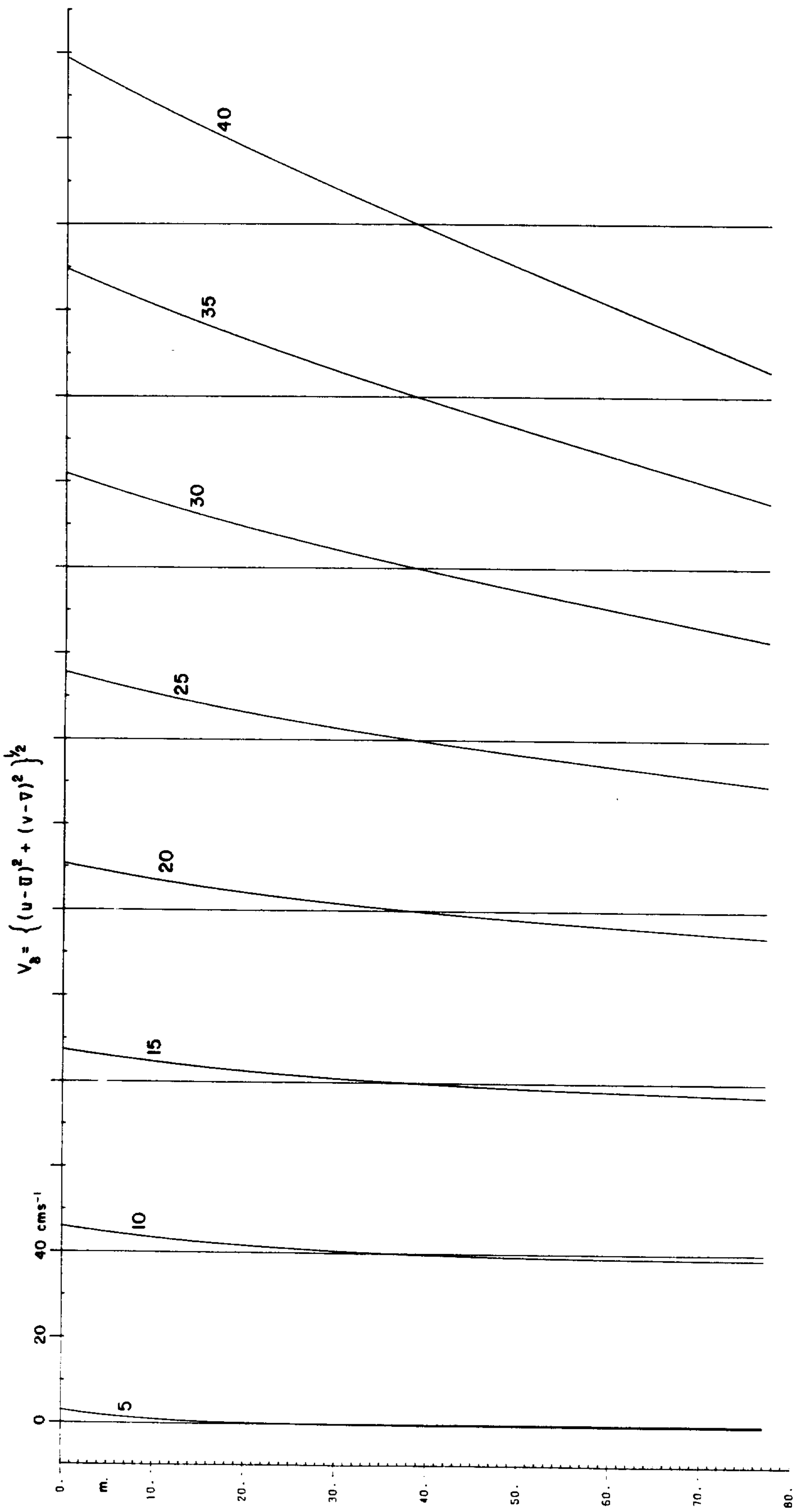

$V_g = \{(u-\bar{U})^2 + (v-\bar{V})^2\}^{1/2}$
40 cms^{-1}
0
20
40
5
10
15
20
25
30
35
40
m.
0.
10.
20.
30.
40.
50.
60.
70.
80.

Figure 4(d)

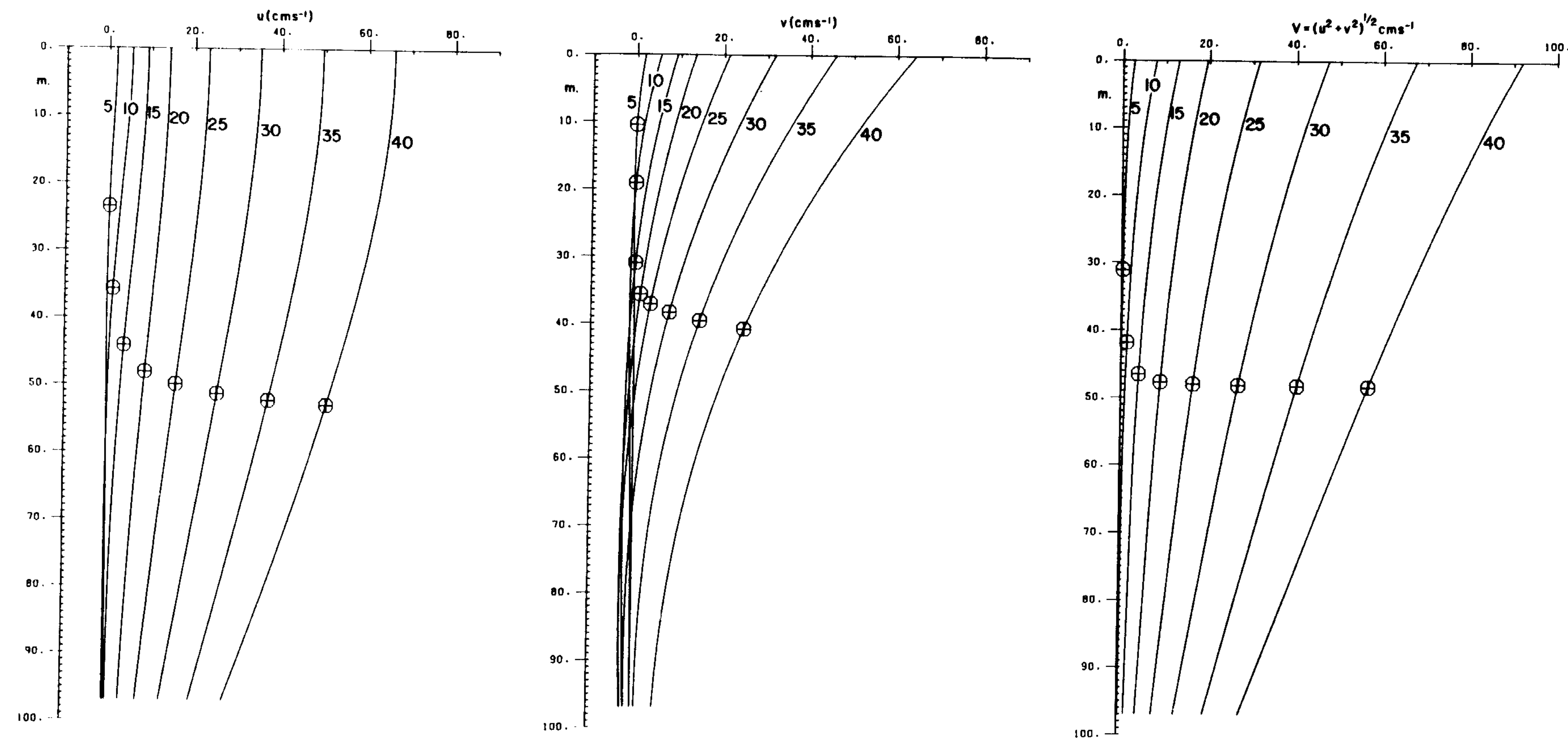

Figure 5 (a)

Figure 5 (a–d). Current profiles at position N_3 ; $\oplus$ denotes the depth-mean; for wind speeds 5 (5) 40 ms^{-1}.

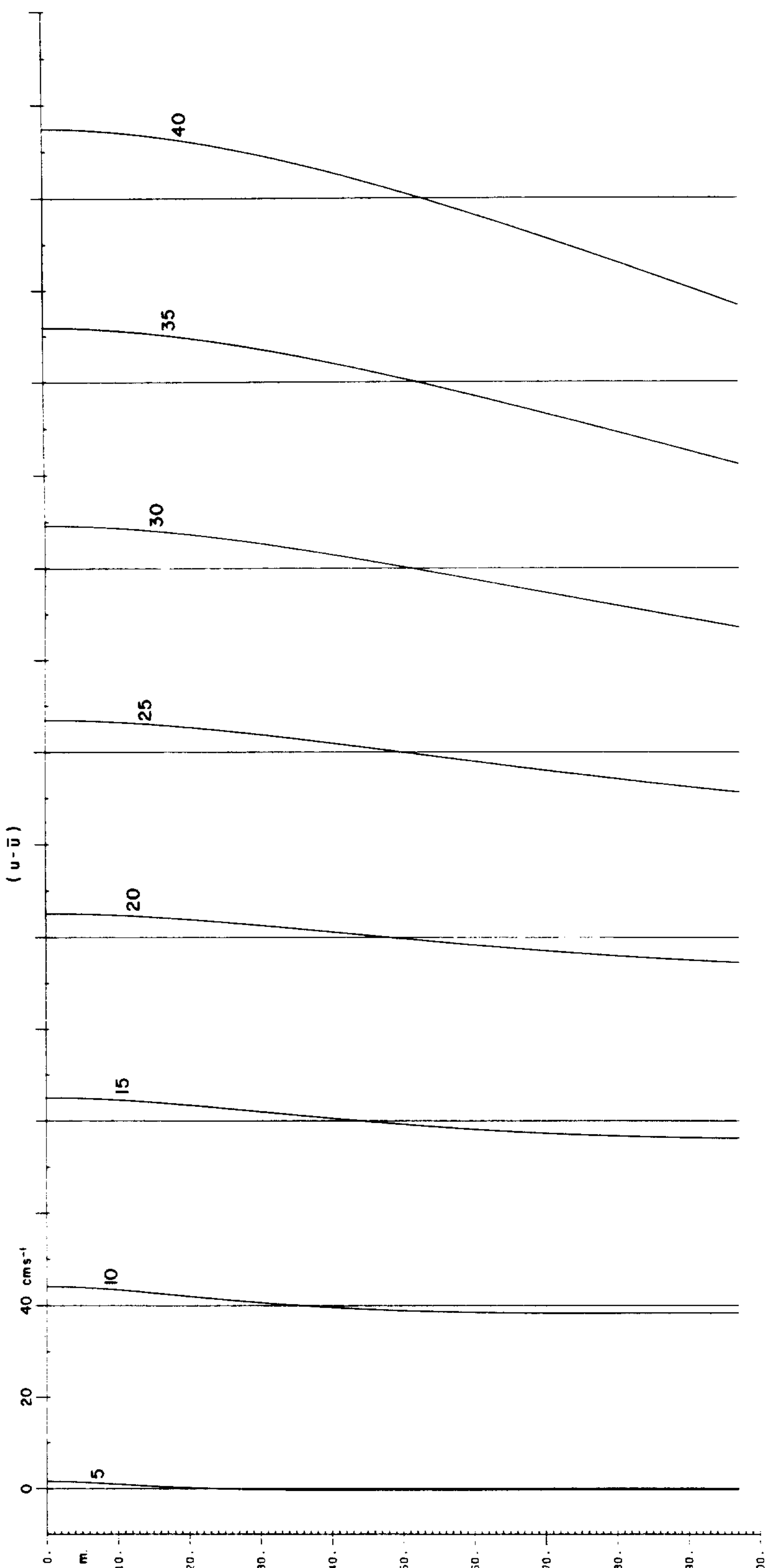

Figure 5(b)

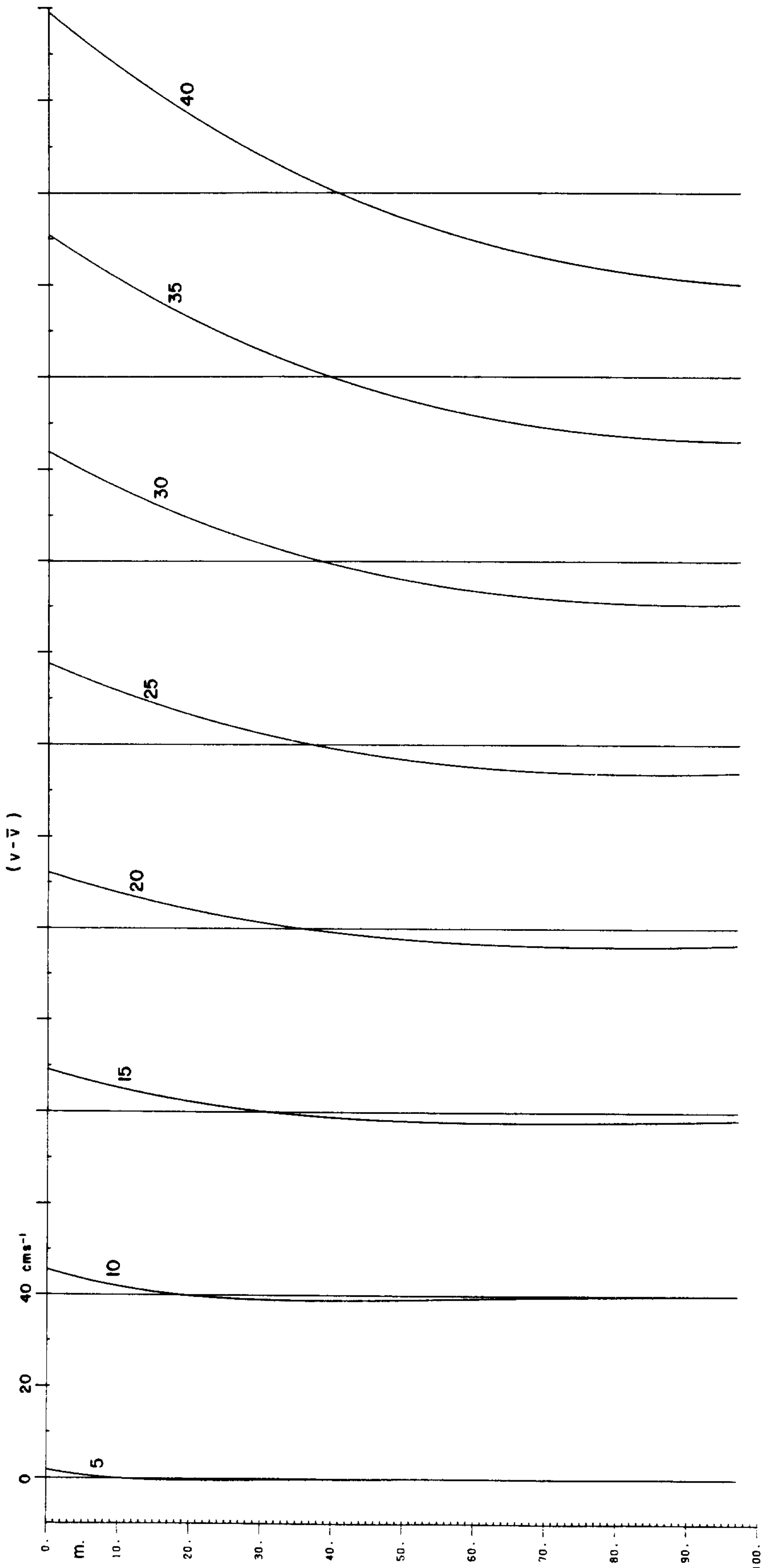
40
35
30
25
20
15
10
5
(v - v̄)
40 cms⁻¹
0
20
40
m.
0.
10.
20.
30.
40.
50.
60.
70.
80.
90.
100.

Figure 5(c)

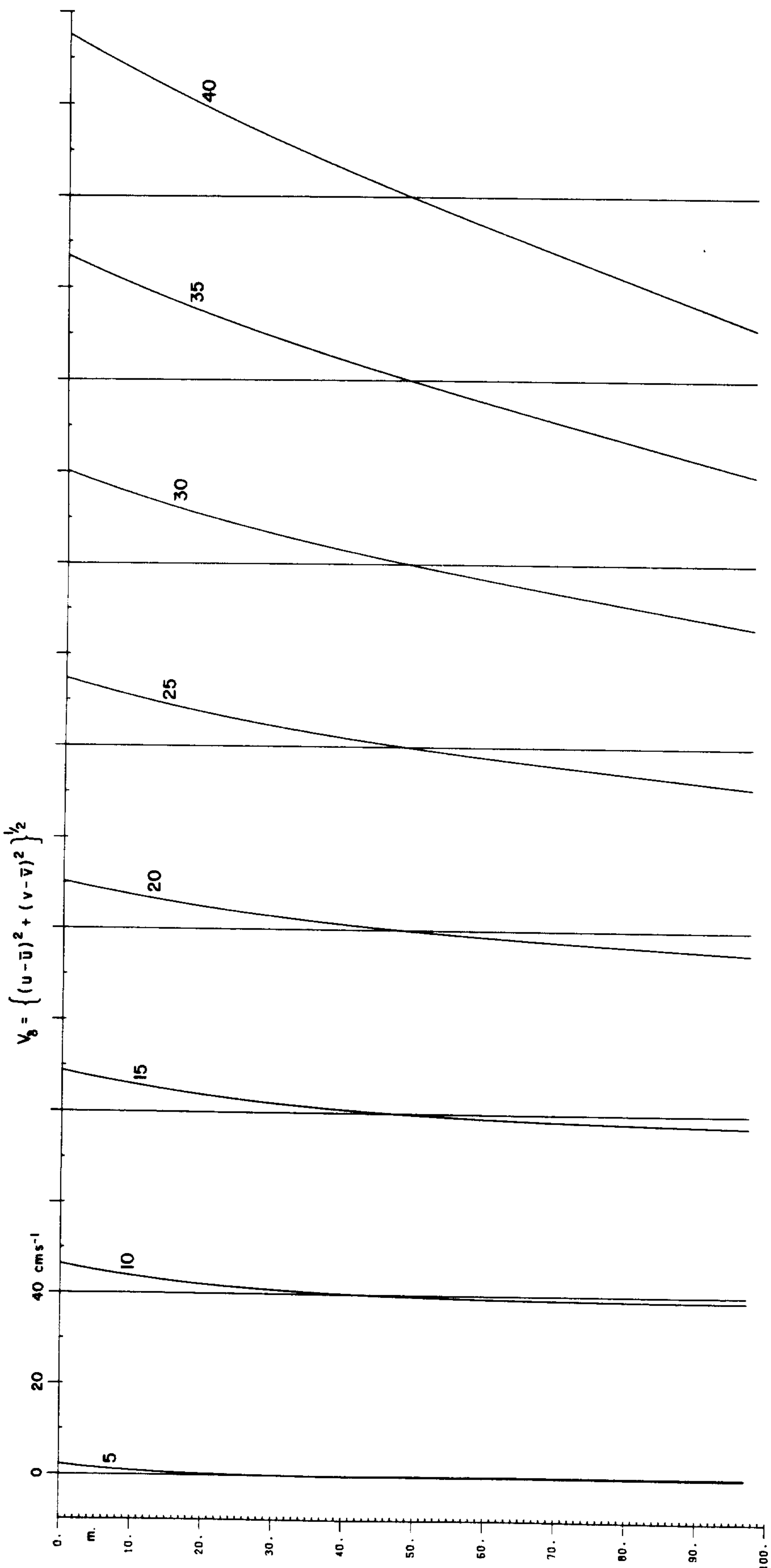

V_s = {(u-ū)² + (v-v̄)²}^½
40 cms⁻¹
0
20
40
m.
0.
10.
20.
30.
40.
50.
60.
70.
80.
90.
100.
5
10
15
20
25
30
35
40

Figure 5(d)

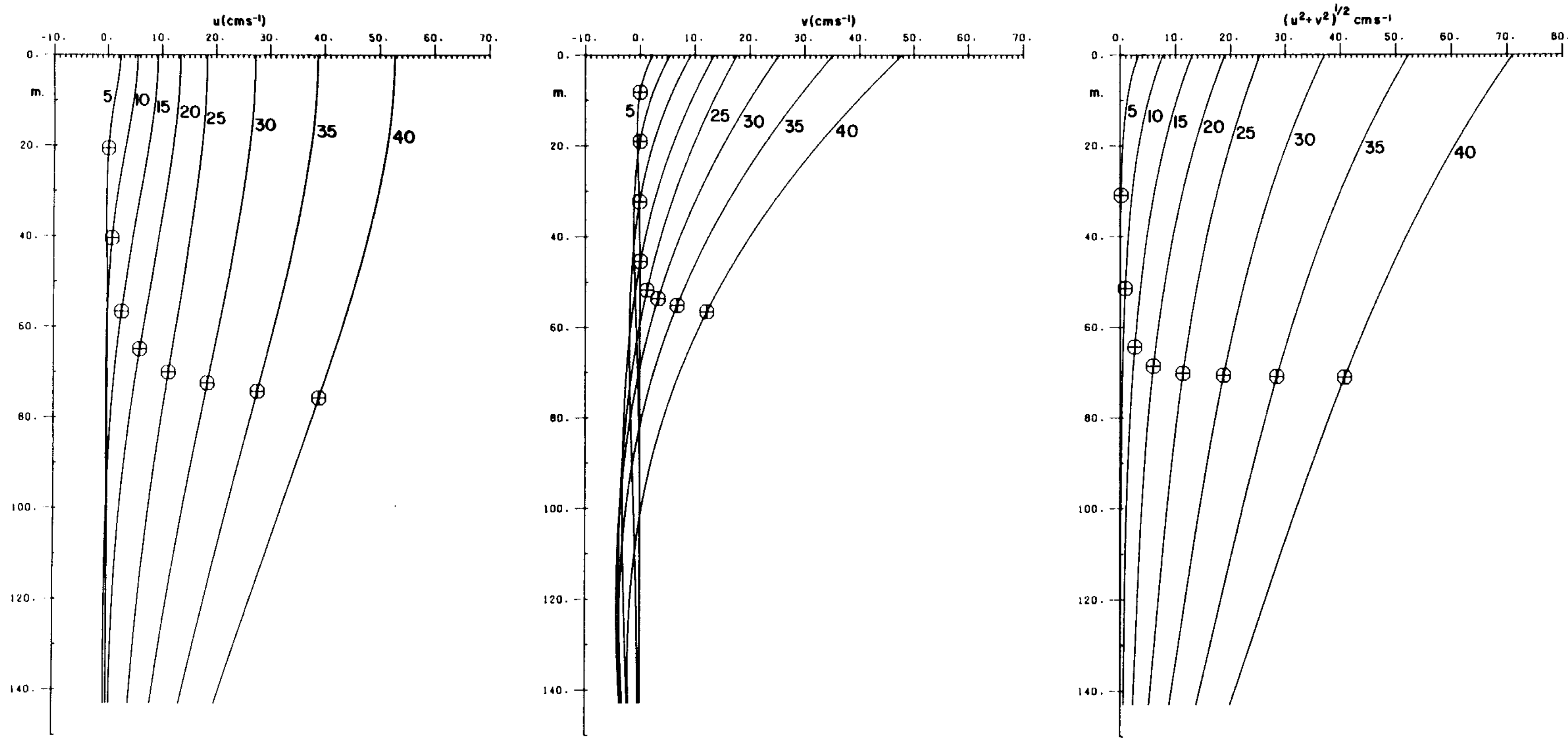

Figure 6 (a)

Figure 6 (a- d) Current profiles at position N_4 ; ⊕ denotes the depth-mean; for wind speeds 5 (5) 40 ms^{-1}.

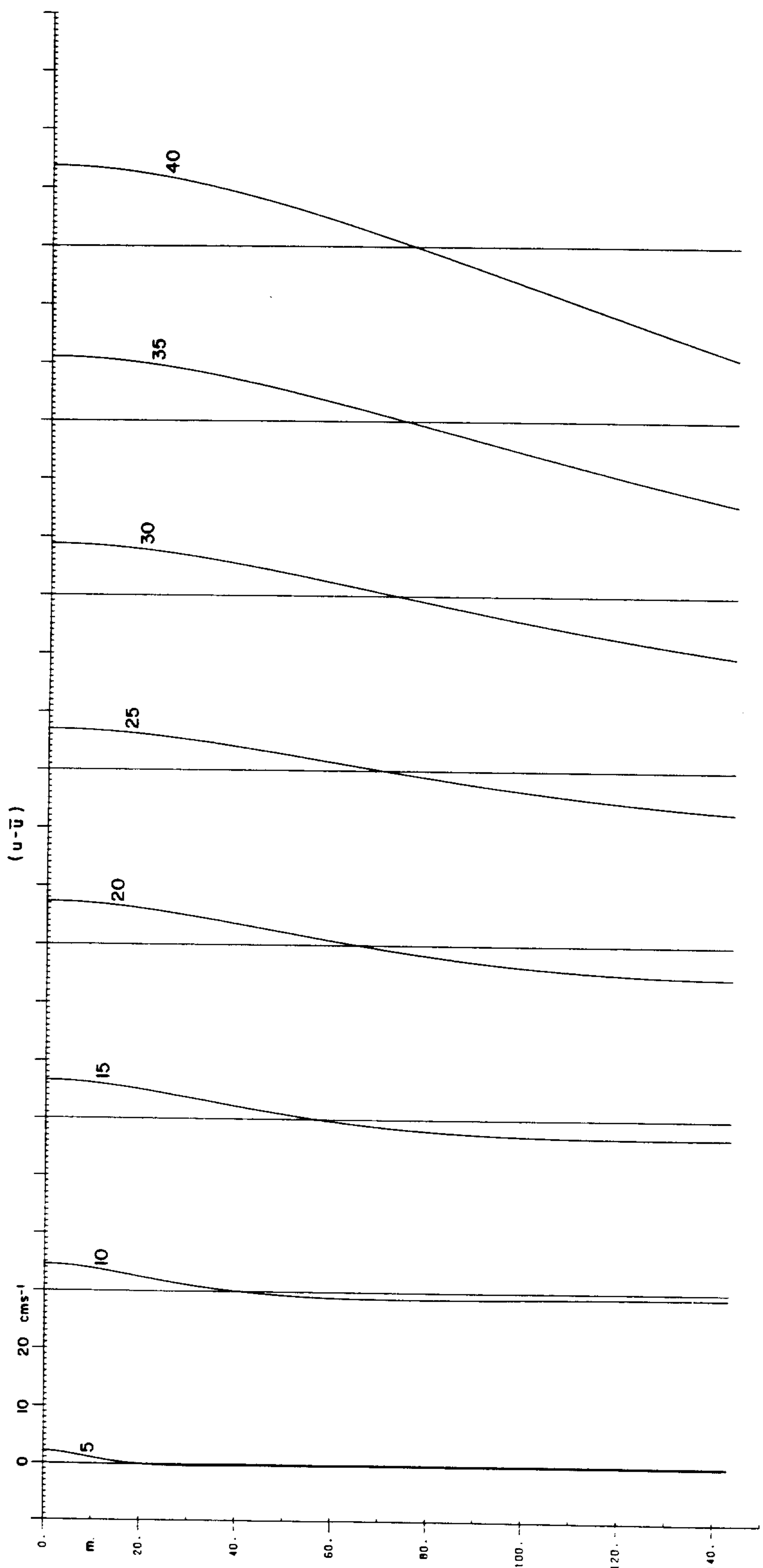

Figure 6(b)

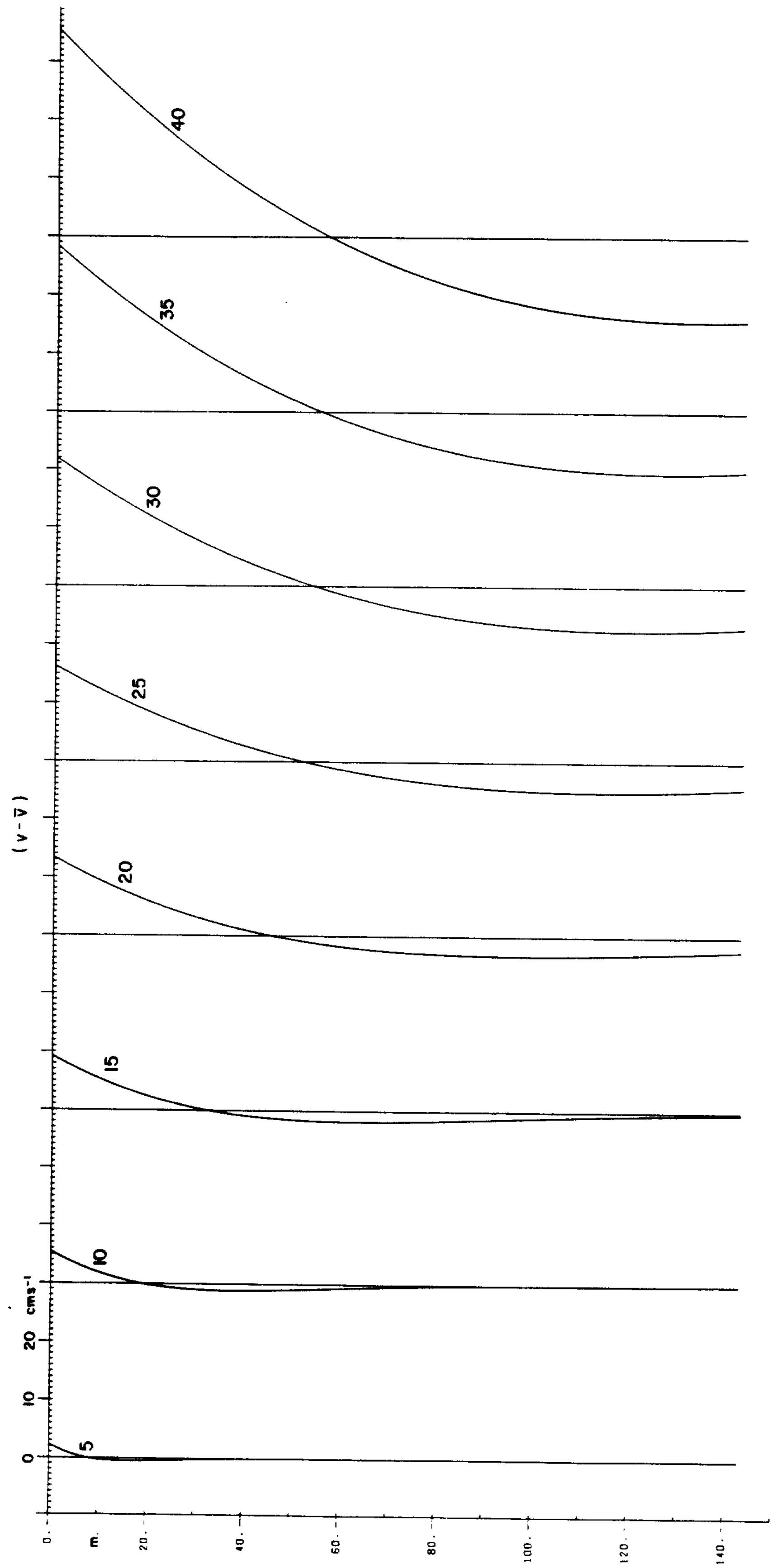

Figure 6(c)

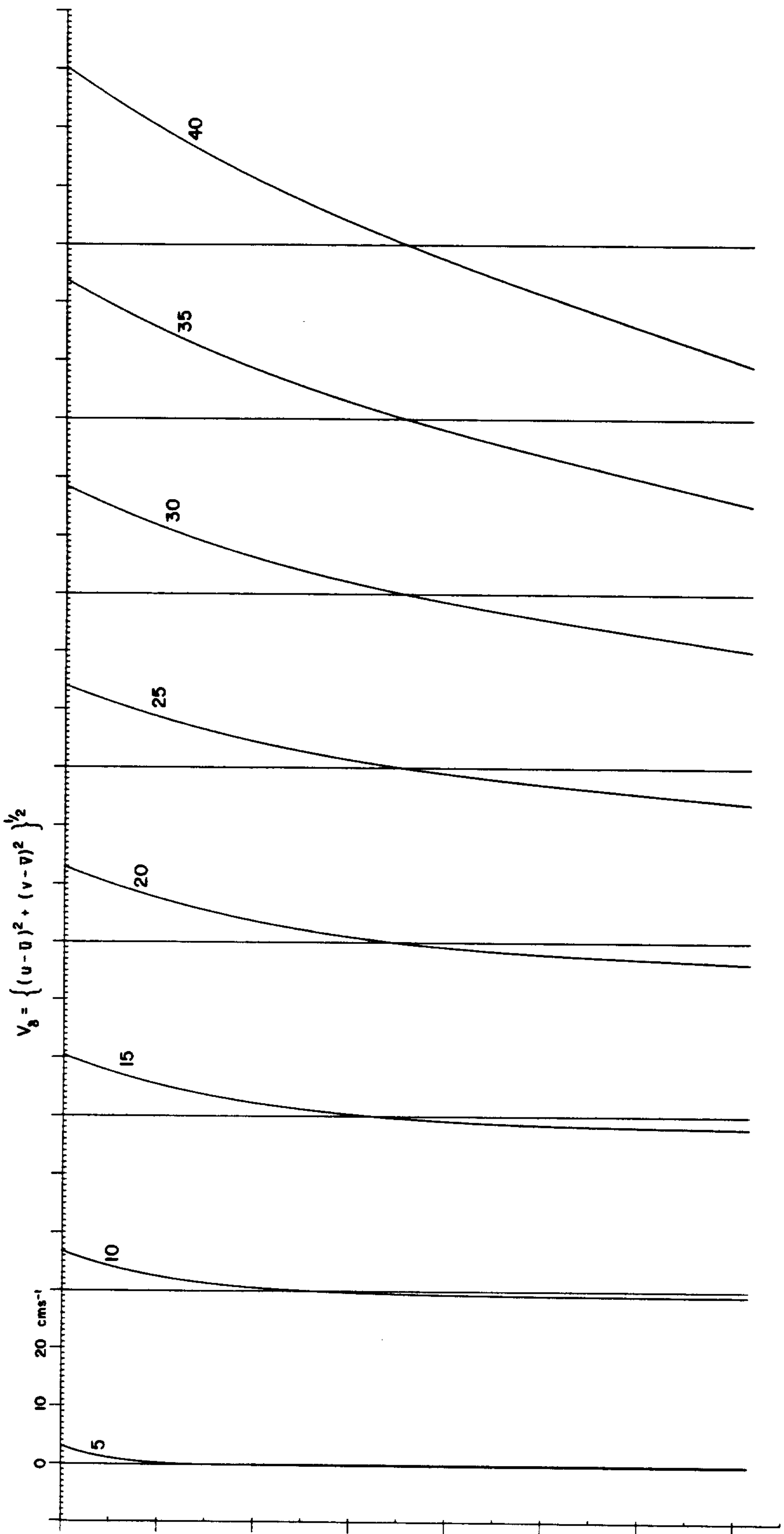
$V_8 = \{(u-\bar{u})^2 + (v-\bar{v})^2\}^{1/2}$
0
10
20 cms⁻¹
m.
0.
20.
40.
60.
80.
100.
120.
140.
5
10
15
20
25
30
35
40

Figure 6(d)

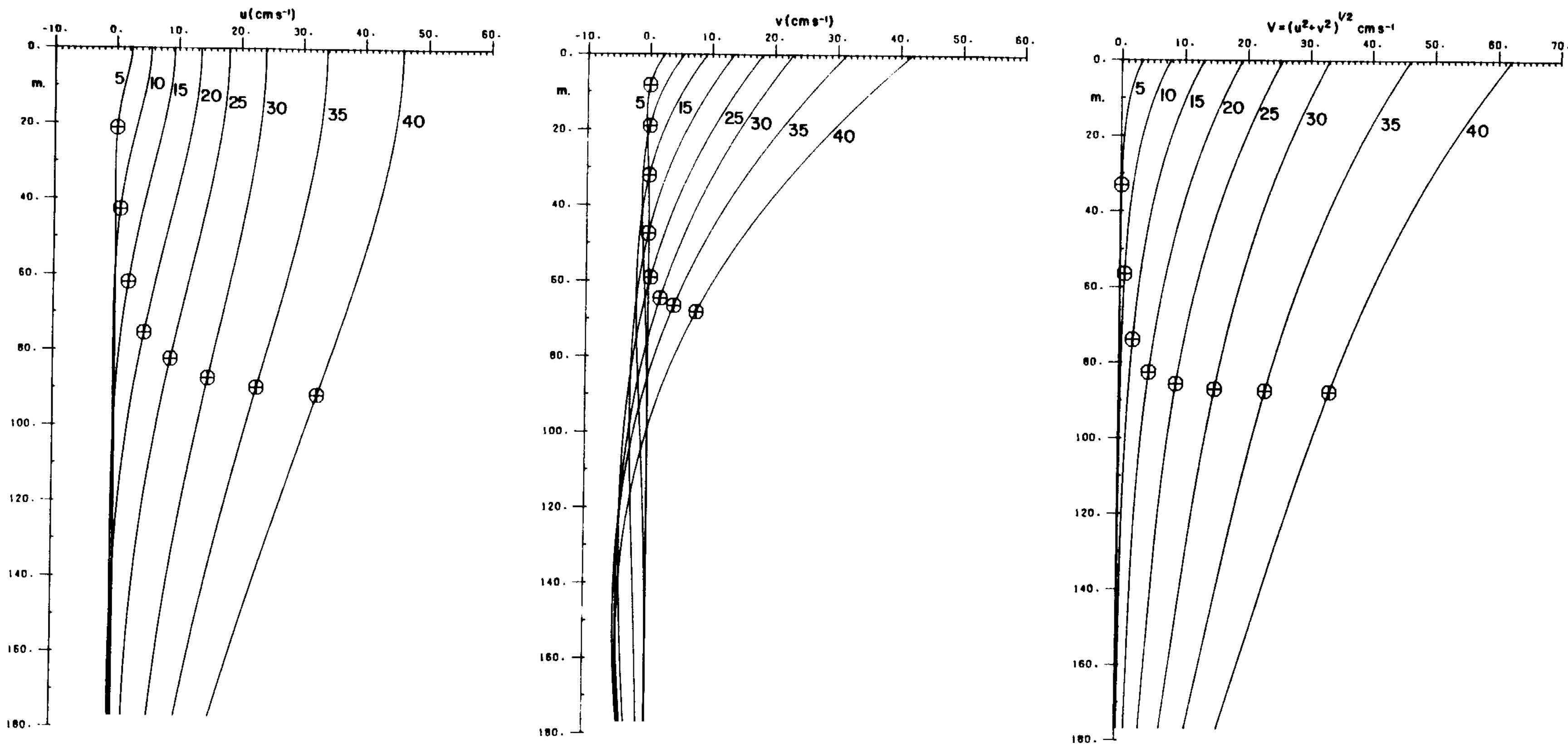

Figure 7 (a)

Figure 7 (a - d) Current profiles at position N_5 ; ⊕ denotes the depth-mean; for wind speeds 5 (5) 40 ms^{-1}.

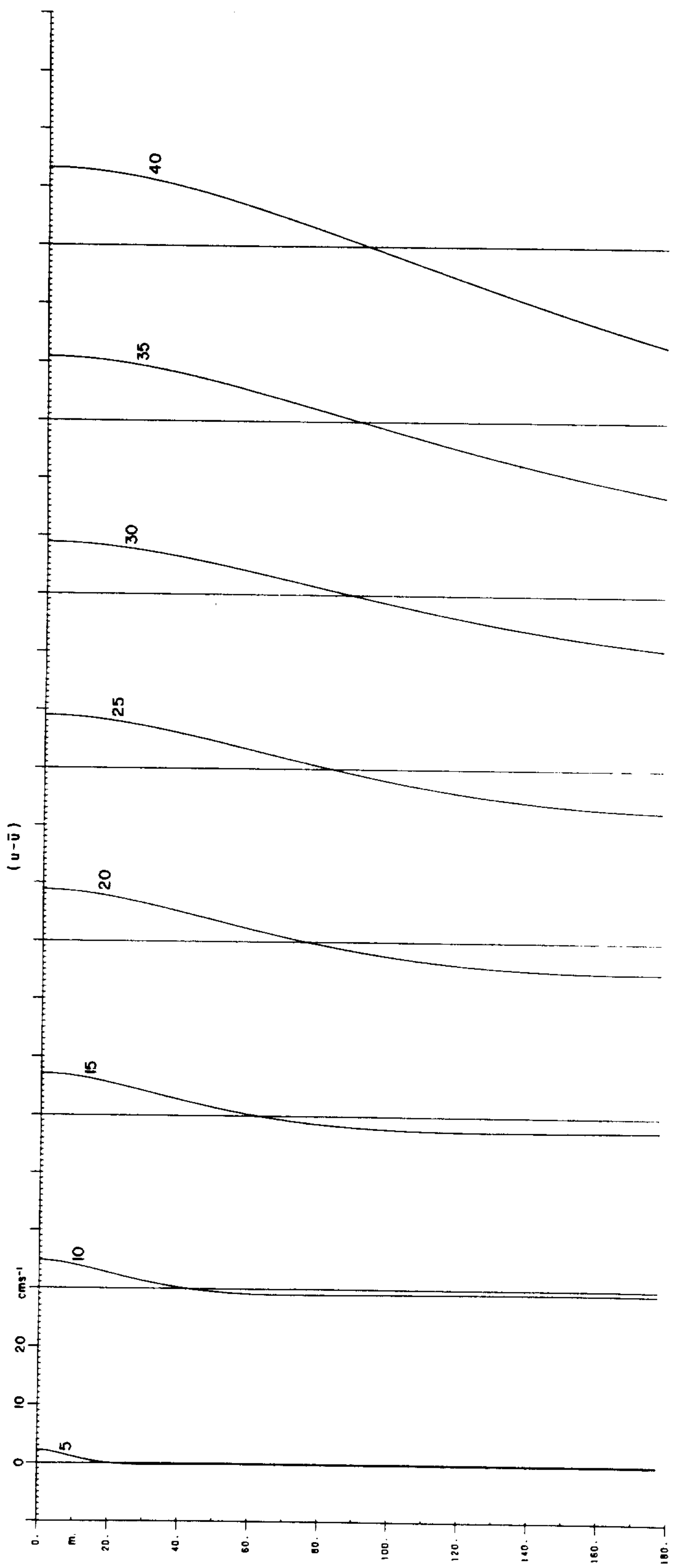
40
35
30
25
20
15
10
5
(u-ū)
cms⁻¹
0
10
20
0.
m
20.
40.
60.
80.
100.
120.
140.
160.
180.

Figure 7(b)

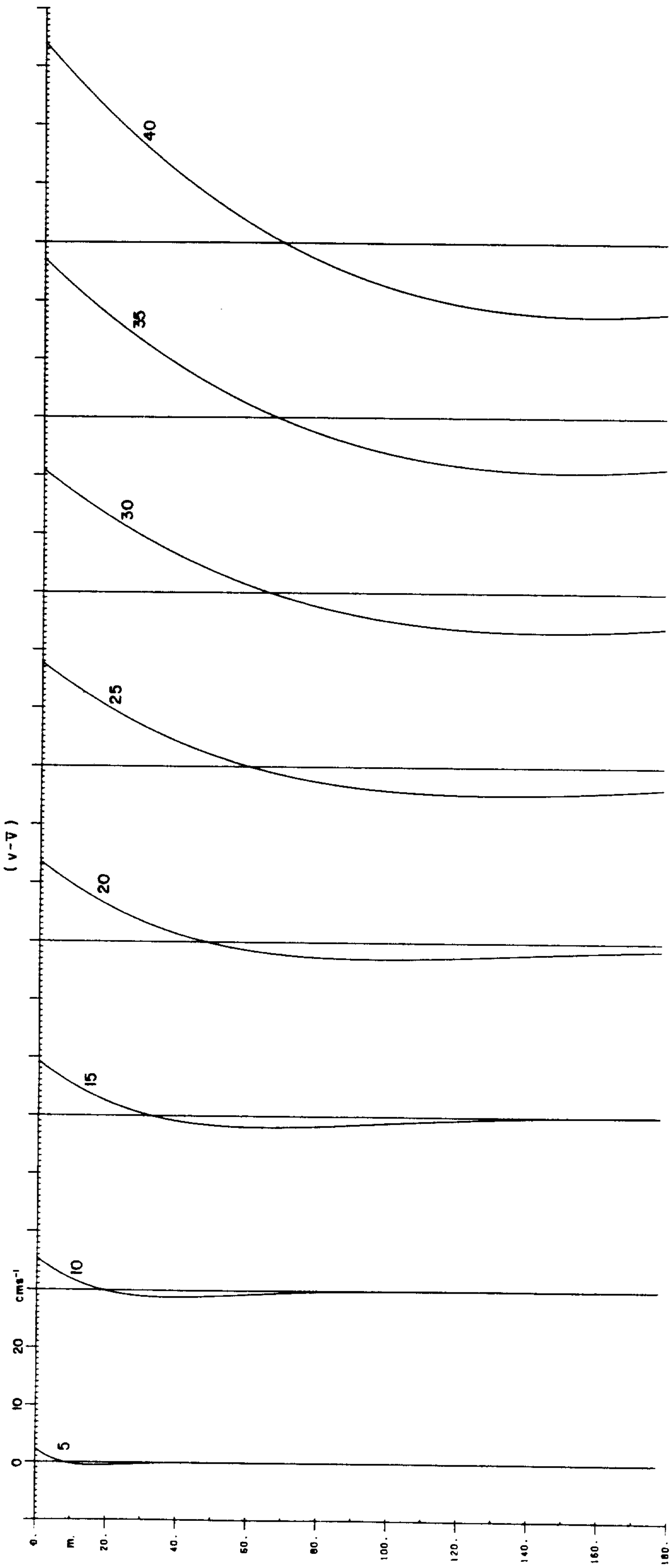
40
35
30
25
20
15
10
5
(v-V̄)
cms⁻¹
0
10
20
0.
m.
20.
40.
60.
80.
100.
120.
140.
160.
180.

Figure 7(c)

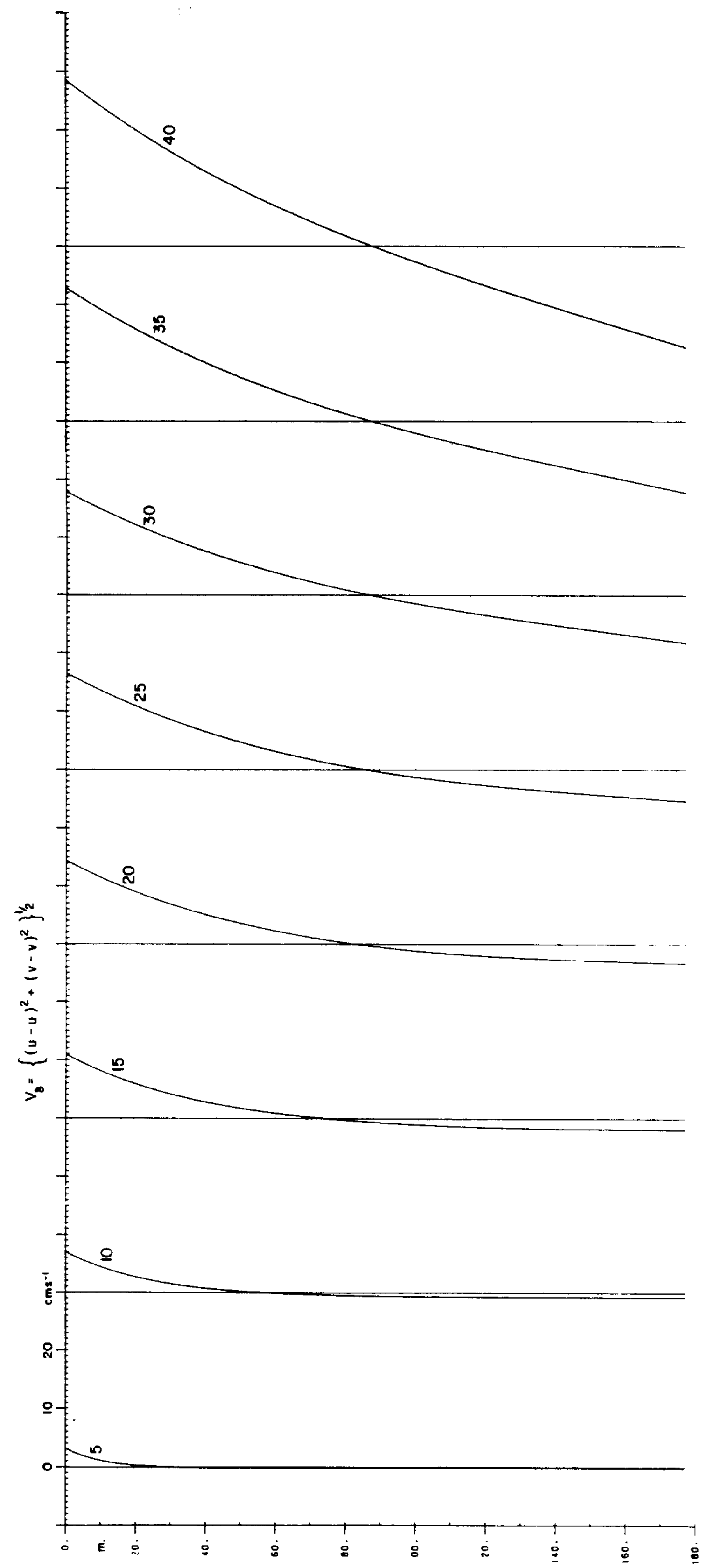

Figure 7(d)

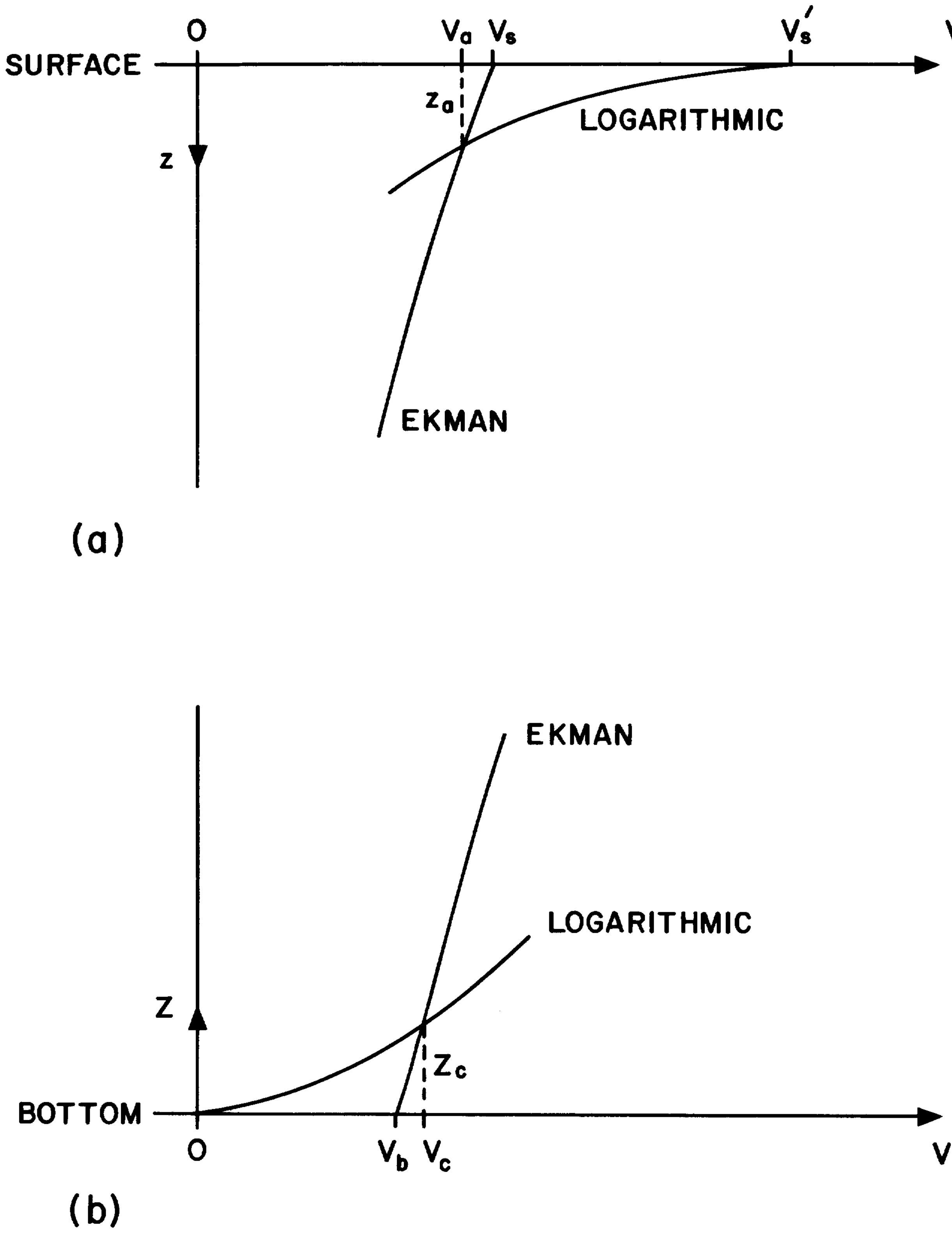

Figure 8. Diagrammatic representation of the logarithmic boundary layers at (a) the sea surface and (b) the sea bed.